2022-08

Swaps in Energy Commodities Markets

McGillivray, Joshua

UNIVERSITY OF CALGARY

Swaps in Energy Commodities Markets

by

Joshua Manfred McGillivray

A THESIS
SUBMITTED TO THE FACULTY OF GRADUATE STUDIES
IN PARTIAL FULFILMENT OF THE REQUIREMENTS FOR THE
DEGREE OF MASTER OF SCIENCE

GRADUATE PROGRAM IN MATHEMATICS AND STATISTICS

CALGARY, ALBERTA
AUGUST, 2022

Abstract

In this paper, we discuss and value variance, volatility, covariance, and correlation swaps in the Vasicek, Schwartz one-factor, and Heston models using a continuous-time regime. The data used is primarily 2019 natural gas and crude oil futures closing prices due to the liquidity and size of the options market in the commodity energy sector. We derive approximations for covariance and correlation swap fair strikes in the Heston model following the continuous time regime, using the discrete regime for reference. We check the accuracy of our approximation using simulated error distributions of the calibrated parameters from the CIR component of the Heston model. We present the effect of varied parameters on the value of the fair strikes for covariance and correlation swaps. Finally, we evaluate the fair strikes of covariance and correlation swaps using three different approximations, yielding values and error bounds of dramatically varying sizes, demonstrating the limitations of the GARCH(1,1) calibration of the Heston model.

Acknowledgments

First and foremost, I thank Professor Anatoliy Swishchuk for his helpful guidance, support, and wisdom throughout my degree. I thank Luca Lalor for his insight into algorithmic trading strategies. Next, I thank my brother for his support and input on this work and the rest of my family for their encouragement. Since this thesis was typeset using LaTeX using the package `ucalgarymthesis`, itself based on the `memoir` class, I would like to thank Don Knuth, Leslie Lamport, Peter Wilson, and Richard Zach. I extend additional thanks to Kyler Kutash, Martijn De Loos, Nicholas David, Kat Smith, Jeremy Bean, Mary Pastyreva, and Racheal Windhorst for their unyielding support, consoling and motivating me through the passing of my father, which allowed me to continue progress on my degree.

To my father, Brent McGillivray whose influence has instilled a burning passion for knowledge and a deep respect for the sciences and all those who contribute to it.

Table of Contents

"One of the many issues bedevilling investment is that the variances and covariances of currencies are unstable over time."

RISK Magazine,
Introducing the Covariance Swap

Chapter 1

Introduction

Variance swaps are common in everyday trading. They are a useful tool in hedging or trading variance directly instead of relying on replicating portfolios or indirect methods. The arbitrage-free valuation of variance swap fair strikes has existed for some time, but the valuation of other similar swaps is still relatively young. The fair strike for volatility swaps was approximated by Brockhaus and Long only 22 years ago in the year 2000 [2]. The market for covariance and correlation swaps is even more untapped. Currently, very little work has been done on the pricing of these swaps. Although there are two indices which track volatilities, the CBOE Volatility Index and the Crude Oil Volatility Index (tickers VIX and OVX respectively), there are no indices which track correlation directly. There are indices which track implied correlation for SPX with rotating tickers $ICJ, $KCJ, and $JCJ; and an implied correlation index with ticker CORE3M. None of the aforementioned indices are useful for correlation swap valuation in commodity energy markets since they focus on the implied correlation of the market as a whole. This paper aims to contribute to the pricing of covariance and correlation swap fair strikes in energy commodity markets, as well as provide more insight into the valuation of these swaps in the Heston model using a continuous-time regime. We begin with a brief history of variance,

volatility, covariance, and correlation swaps in quantitative finance.

Before any of these swaps could be discussed, the notion of stochastic volatility needed to be created. This was done by Hull and White in 1987 in the context of European options [13]. Demeterfi, et al. in 1999 marked the birth of variance and volatility swaps with a thorough explanation of the theory behind them [7]. In their paper, they created a replicating portfolio for volatility swaps using variance swaps. Brockhaus and Long in 2000 created a useful approximation which can be used to price volatility and variance swaps directly [2]. Also in 2000, Heston and Nandi created closed-form formulae for the value of volatility swaps which depended only on observable variables. In the same paper, they showed how one can hedge different volatility derivatives by trading only in the underlying asset and a risk-free asset, mitigating substantial transaction costs [11]. An analytic solution for volatility swap pricing was found by Theoret et al. in 2002 [26]. In 2004, Swishchuk proposed a probabilistic approach for the pricing of variance and volatility swaps in the Heston model [24]. In the same paper, Swishchuk also gave an approximation for the discrete covariance and correlation between two stocks. The approaches in Swishchuk's paper are central to this paper. In 2006, Windcliff et al. developed a hedging strategy for volatility derivatives with a focus on small fixed positions in vanilla options, avoiding some of the drawbacks of a delta hedge [28]. In 2007, Elliott et al. developed a model for pricing volatility and variance swaps under a continuous-time Markov-modulated version of the Heston stochastic volatility model [9]. Carr and Lee created strategies to hedge variance and volatility using the corresponding swaps with mean absolute hedging errors below 10% in 2007 [3]. In 2008, Sepp priced options on realized variance in the Heston model with jumps in returns and volatility [22]. In 2009, Carr and Lee provided an overview of the current market for variance and volatility swaps as well as provided some fundamental results related to these swaps [4]. Trolle and Schwartz published a paper in 2010 investigating

variance risk premia in energy commodities markets and found the return profile of a natural gas variance swap resembles that of a call option, and with crude oil, that of a put option [27]. Also in 2010, Swishchuk priced variance and volatility swaps in the energy market using the Brockhaus-Long approximation (B-L approximation) for an asset whose stochastic volatility follows the continuous time GARCH(1,1) model [25]. In 2010 Jacquier and Shaoui explained the spread between correlation swap strikes and implied correlation was due to the volga (that is, the second partial derivative with respect to σ) of the dispersion trade [15]. In 2011, Da Fonseca et al. showed how variance swaps can implicitly span covariance risk and that the impact of covariance risk on optimal investment strategies can be large [6]. In 2013, Salvi and Swishchuk approximated covariance and correlation swap fair strikes using Markov-modulated volatilities [20]. Chunhawiksit and Rujivan derived a closed form pricing formula for discretely sampled variance swaps in the Schwartz two-factor model while including stochastic convenience yields and seasonality in 2016 [5], [21]. Finally, in 2021 Rujivan analytically priced discretely sampled variance swaps in commodity derivative markets by solving the problem in the context of the solution to a partial differential equation [18].

It appears—as of the writing of this paper—that very few others have worked on the valuation of variance, volatility, covariance, and correlation swaps in energy commodity derivatives markets. The focus of this paper on energy commodity markets is based on the liquidity and size of these markets. The energy sector dominates every other commodity combined. Consider two important indices: S&P GSCI and DJ-AIGCI (Note that the DJ-AIGCI is known as the Bloomberg Commodity Index, BCOM as of 2014). Crude oil and natural gas are the two largest contributors to both of these indices.

For the S&P GSCI, the weight of each of their 24 tracked commodities is determined by world production over 5 years. In 2007 the weight of

crude oil was 51.30% and 6.71% for natural gas. For the DJ-AIGCI (i.e. BCOM) the weightings of each of their 19 commodities are determined by the liquidity and world production. The weighting of crude oil was 13.88% and natural gas was 11.03% in 2007 [25].

Indeed, in 2020 the S&P GSCI had the reference percentage sector weight of the energy sector at 61.71%. The next largest weighting was agriculture at 15.89% and in third, industrial metals at 10.65% [19]. This fell slightly in 2021, but the energy sector still dominates nonetheless. The large worldwide demand for natural gas and crude oil leads to one of the most liquid derivatives markets available for any commodity. Naturally, a large fluctuation in crude oil prices will dictate a large fluctuation in these commodity indices. Since a significant use for swaps is in hedging, it follows that research in commodity markets with an emphasis on the energy sector should prove fruitful for investors.

There are six major datasets used in this paper. They are:

1. 1 year of daily 2018 natural gas front month futures closing prices,
2. 1 year of daily 2019 natural gas front month futures closing prices,
3. 1 year of daily 2018 crude oil front month futures closing prices,
4. 1 year of daily 2019 crude oil front month futures closing prices,
5. 3 years of daily 2017-2019 CBOE volatility index (VIX) closing prices,
6. 1 year of daily 2019 crude oil volatility index (OVX) closing prices.

Data sets 1–4 are obtained via the Market Watch website (https://www.marketwatch.com/). Data sets 5 and 6 are downloaded from Yahoo Finance (https://ca.finance.yahoo.com/). We did not use newer data because as of the formulation of this thesis, the ongoing COVID-19 pandemic continues as a black swan event. Supply chain shocks will take time to fade and thus data from 2020 onwards may not be an accurate depiction

of usual trends in these markets. To avoid inaccuracies brought on by this unprecedented time, we took data from before the pandemic. The 2019 data sets are the primary focus of this paper, with the 2018 and VIX data sets being used to supplement section 3.2 with additional data. We note that data sets 1–4 needed to be sorted from oldest to newest to maintain the chronology of the data.

This paper is divided into four major parts, each with several chapters and sections. Part I is dedicated to an already present approximation for continuous time variance and volatility swap fair strike prices for both the 2019 crude oil and the 2019 natural gas data sets. The realized discrete variance, volatility, covariance, and correlation for both 2019 data sets is also present and used for reference. This part's calculations follow the Heston model defined for $i = 1, 2$ under the risk-neutral measure Q by

$$\begin{cases} \frac{dS_t^i}{S_t^i} = r_t^i dt + \sigma_t^i dw_t^i, & i = 1, 2, \\ d(\sigma_t^i)^2 = k_i(\theta_i^2 - (\sigma_t^i)^2)dt + \gamma_i \sigma_t^i dw_t^j, & j = i + 2. \end{cases} \tag{1.1}$$

With $k_i = k_i^* + \lambda_i$, $\theta_i^2 = k_i^* \theta_i^* / (k_i^* + \lambda_i)$, and $\lambda_i \in \mathbb{R}$ is the market price of risk. Part II discusses the models used for our 2019 data set. Sections 4.1–4.5 cover the Vasicek process for $i = 1, 2$ defined under the risk-neutral measure Q by

$$dS_t^i = a_i(b_i - S_t^i)dt + \sigma_i dw_t^i$$

where $a > 0$, $b = b^* - \lambda\sigma/a$, $w_t^i := B_i(t) + \lambda t$, $B_i(t)$ is a standard brownian motion, and $\lambda \in \mathbb{R}$ is the market price of risk. This model is covered thoroughly from presenting the solution to the Vasicek SDE and deriving the expected value, variance, volatility, covariance, and correlation of assets following the process, to the calibration of the model and its performance relative to the crude oil volatility index. Section 4.6 repeats sections 4.1–4.5 but following the Schwartz one-factor model given in [21]. Section 4.7 compares the performance of the Schwartz one-factor model with the Heston model calculations from Part I. Appendix 8 is a discussion dedicated to the

performance of the calibration for the Heston model. In this appendix, we show through simulation methods that large errors in the calibration parameters k, θ, and γ are not only possible but frequent and likely. This result is used to help explain the poor performance of the well-vetted Heston model in section 4.7.

Part III relies heavily on results from Swishchuk's 2004 paper [24] and Salvi's 2014 paper [20] to derive approximations for the covariance and correlation between two assets following the Heston model in sections 5.2 and 5.3. A bivariate version of the Brockhaus-Long approximation is derived in 5.2 as well. Section 5.4 goes further to derive an approximation of the risk-neutral expected value of the realized covariance and correlation between these two assets defined by

$$\mathrm{Cov}_R(S^1, S^2) := \frac{1}{T}\int_0^T \mathrm{Cov}(S^1, S^2)dt$$

and

$$\mathrm{Corr}_R(S^1, S^2) := \frac{\mathrm{Cov}_R(S^1, S^2)}{\sqrt{(\sigma_R^1)^2}\sqrt{(\sigma_R^2)^2}}$$

respectively. This yields an approximation for the fair strikes for covariance and correlation swaps. A small discussion on the error of one of the approximations is included.

Lastly, Part IV contains a sensitivity analysis in chapter 6. The parameters of the Heston model are varied around their likely errors determined in section 8 while holding the others constant. This yields us a valuable intuition that aids us in chapter 7. Chapter 7 combines the results from parts II and III to give numerical values for the covariance and correlation fair strikes between natural gas and crude oil. In total, three approximations are given with varying accuracy using informed decisions from the results in appendix 8 and chapter 6.

The chapters of this paper are arranged as follows: Chapter 2 applies the methods of Swishchuk from [24] to determine the variance and volatility

swap fair strikes in continuous-time and realized variance, volatility, covariance, and correlation in discrete time to the 2019 natural gas and crude oil datasets mentioned above. Chapter 3 uses the Augmented Dickey-Fuller and Phillips-Perron tests, visual assessment, and an algorithmic trading strategy to determine if spot prices are mean-reverting or random walks. Chapter 4 verifies that the Heston model is a good model to use for crude oil and natural gas swap valuation by using it, the Vasicek, and the Schwartz one-factor models to find volatility swap fair strikes and then comparing them to the OVX. Chapter 5 develops the main theoretical results of this paper; covariance and correlation swap fair strikes in the continuous-time Heston regime. Chapter 6 is a sensitivity analysis of how k, θ, and γ affect the correlation and covariance fair strike valuations. Chapter 7 combines the results from chapters 5, 6, and appendix 8 to create three approximations for the fair strikes of the covariance and correlation swaps between crude oil and natural gas in the 2019 data set. We created three approximations to illustrate how varying the number of terms in the approximation can dramatically affect the valuation and uncertainty of the fair strikes.

Part I

Previous Results in Swaps

Introduction

In this part, we will perform six different calculations in the continuous and discrete regimes for both natural gas and crude oil:

1. discrete realized variance,
2. discrete realized volatility,
3. discrete realized covariance,
4. discrete realized correlation,
5. continuous expected realized variance swap,
6. continuous expected realized volatility swap.

Each of which will be determined using the methods presented by Swishchuk in [24] following the Heston model. We will solve these problems in order by applying them to one year of daily front-month natural gas and crude oil futures from January 1st, 2019 until December 31st, 2019. Specifically, the two datasets being considered will be "Crude Oil WTI (NYM $/bbl) Front Month" futures and "Natural Gas (NYM $/mmbtu) Front Month" futures. We will also discuss the use of the Heston model for the price and volatility processes and assess whether the assumptions made by the model are valid in this context.

The general equation for the payoff, P, of a swap is

$$P_T = N(\Gamma_T - K_\Gamma).$$

Where N is the notional amount, Γ_t is the floating leg of the contract with regards to the underlying asset (e.g. variance, volatility, etc.). K_Γ is a constant; specifically, it is the fixed leg or the strike of the contract. The subscript Γ is to emphasize the strike is in units of Γ and so it may be differentiated from other strikes that may appear. For contract valuation we must work with a similar equation:

$$P_T = Ne^{-rT}(\mathrm{E}(\Gamma_T) - K_\Gamma).$$

Where r is the risk-free interest rate, T is the duration of the contract in years, and the expectation is taken with respect to the risk-neutral measure. Since swaps are forward price processes, we can solve for the fair strike of the contract easily by setting $P = 0$:

$$\begin{aligned} 0 &= Ne^{-rT}(\mathrm{E}(\Gamma_T) - K_\Gamma) \\ 0 &= E(\Gamma_T) - K_\Gamma \\ K_\Gamma &= \mathrm{E}(\Gamma_T). \end{aligned} \tag{1.2}$$

Therefore, to find the fair strikes for variance, volatility, covariance, and correlation swaps, we simply need to find the expected values of the contracts' floating legs. Unfortunately, for now the expected value of the contracts' floating legs are currently out of reach for items 2, 3, and 4 listed above. The expected value of items 2, 3, and 4 is attainable with some work but this is not the subject of this paper. The expected value for item 1 is given by Swishchuk in [24] but requires some work to be implemented in this numerical example, thus for items 1–4 we will calculate their discretely sampled realized values instead of their fair strike values. This means that items 1–4 are not swap valuations, but rather, they are heuristics to tell if the swap valuations of contracts 5–6 are reasonable. The realized values for

items 1 and 2 can be used to compare the effectiveness of the valuations in the continuous regime for contracts 5 and 6. Items 3 and 4 will be a point of comparison towards the end of this paper after the theory and valuation of the fair strikes for the continuous-time covariance and correlation swaps are determined. Since each dataset is a year of daily data, there are plenty of data points for the discrete regimes to converge and should represent the relevant values accurately.

Chapter 2

Discrete and Continuous Valuation of Variances, Volatilities, Covariances, and Correlations

2.1 Valuation of discretely sampled natural gas futures' variance and volatility

The discretely sampled realized variance and volatility of the natural gas dataset is a straightforward application of a formula given in [24]:

$$\mathrm{Var}_n(S_{NG}) := \frac{n}{T(n-1)} \sum_{i=1}^{n} \ln^2 \left(\frac{S_{NG,t_i}}{S_{NG,t_{i-1}}} \right).$$

Where n is the number of data points in our dataset, T is the length of the contract in years, and S_{NG,t_i} is the price of natural gas at time $t_i \in [0, T]$. For the provided data $n = 254$. Applying this formula using Excel we arrive at

$$\mathrm{Var}_n(S_{NG}) = 0.181172306.$$

Fortunately, the discrete realized volatility is easy to calculate as it is the square root of $\mathrm{Var}_n(S_{NG})$:

$$\mathrm{Vol}_n(S_{NG}) := \sqrt{\mathrm{Var}_n(S_{NG})} = 0.425643403.$$

2.2 Valuation of discretely sampled covariance and correlation

The method of computing the discretely sampled realized covariance and correlation is very similar to the previous section but requires the volatility of both the crude oil and natural gas processes. The natural gas realized volatility is given in the previous section. Following the same process we arrive at the crude oil variance and volatility:

$$\mathrm{Var}_n(S_{oil}) = 0.114034599, \tag{2.1}$$

$$\mathrm{Vol}_n(S_{oil}) := \sqrt{\mathrm{Var}_n(S_{oil})} = 0.337690093. \tag{2.2}$$

Now, we may approximate the realized covariance between the natural gas and crude oil futures with another formula given in [24],

$$\mathrm{Cov}_n(S_{NG}, S_{oil}) := \frac{n}{T(n-1)} \sum_{i=1}^{n} R_i^{NG} R_i^{oil}$$

where

$$R_i^j = \ln\left(\frac{S_{j,t_i}}{S_{j,t_{i-1}}}\right) \text{ for } j = NG, oil.$$

Inputting this formula into Excel yields the approximate realized covariance between the futures:

$$\mathrm{Cov}_n(S_{NG}, S_{oil}) = 0.022832512.$$

Finally, we must approximate the correlation with

$$\mathrm{Corr}_n(S_{NG}, S_{oil}) = \frac{\mathrm{Cov}_n(S_{NG}, S_{oil})}{\mathrm{Vol}_n(S_{NG})\,\mathrm{Vol}_n(S_{oil})}.$$

Using this formula we arrive at our approximation for realized correlation:

$$\text{Corr}_n(S_{NG}, S_{oil})) = 0.158850823.$$

At first glance, these values are fairly small. This begins to make sense when we carry out 2 simple regressions on the natural gas and crude oil datasets with 1 day lag. The R^2 value for these regressions are $R^2_{oil} = 0.891208551$ and $R^2_{NG} = 0.930689987$. In other words, the vast majority of the movement of crude oil and natural gas is explained by their previous day's price. This regression indicates that the correlation between them is comparatively small since the effects they have on themselves overshadow much of the effects they have on each other.

2.3 Valuation of continuously sampled expected realized variance natural gas and crude oil swaps

Next, we will determine the expected value of the variance and volatility of both natural gas and crude oil using the continuous regime. Let V be the continuously realized variance given by $V = \text{Var}_R(\sigma_t) := \frac{1}{T}\int_0^T \text{Var}(S_s)ds$, then the continuous variance swap is determined in [24] to be

$$\text{E}(V) = \frac{1 - e^{-kT}}{kT}(\sigma_0^2 - \theta^2) + \theta^2,$$

where k is the mean reversion speed, θ is the mean-reverting level, and σ_0^2 is the short-run variance of the relevant dataset. Swishchuk [24] also points out how to calibrate the solution for these parameters using a GARCH$(1, 1)$

model through maximum likelihood estimation:

$$\theta = \frac{C}{(1-\alpha-\beta)dt}, \tag{2.3}$$

$$k = \frac{1-\alpha-\beta}{dt}, \tag{2.4}$$

$$\gamma = \alpha\sqrt{\frac{\xi-1}{dt}}, \tag{2.5}$$

where γ is the volatility of the volatility, ξ is the Pearson kurtosis, $dt = 1/n = 1/254$, and α, β, and C are the ARCH(1) coefficient, GARCH(1, 1) coefficient, and constant term respectively.

Using the MATLAB econometrics toolbox GARCH library to find α, β, and C, as well as calculating equations (2.3), (2.4), and (2.5) in Excel, we have all the needed parameters for the fair strike valuation. These quantities are summarized in Table 2.1. The MatLab code will be left in Appendix 8.

Parameter	Crude Oil	Natural Gas
k	7.9506241	7.4939013
T	1	1
σ_0	0.021161467	0.026680822
θ	0.1140747	0.2068726
γ	1.0490996	3.8696995
α	0.0262925	0.10890697
β	0.9424058	0.86158949
C	0.0000141	0.0000240
dt	1/254	1/254
ξ	7.268077524	5.970607225

Table 2.1: Heston model parameters for one year of daily 2019 crude oil and natural gas futures. The p-values for α, β and C for the crude oil data set are 0.151, $2.24 * 10^{-194}$, and 0.0988 respectively. For the natural gas data set, the p-values are 0.00876, $9.95 * 10^{-44}$, and 0.260 respectively.

The continuous-time expected value of the realized natural gas and crude

oil variances are

$$\mathrm{E}(V_{NG}) = 0.0371836 \text{ and } \mathrm{E}(V_{oil}) = 0.0114332.$$

Note that as per equation (1.2), these values are also the fair strikes of their respective contracts.

2.4 Valuation of continuously sampled expected realized volatility natural gas and crude oil swaps

The valuation of the fair strikes for the crude oil and natural gas volatility swaps is similar to the process in the previous section, however, we must calculate the variance of the realized variance as well, $\mathrm{Var}(V)$. In doing so we may apply the Brockhaus-Long approximation [2] and approximate the fair strike of the volatility swaps:

$$\mathrm{E}(\sigma_R(S)) = \mathrm{E}(\sqrt{V}) \approx \sqrt{\mathrm{E}(V)} - \frac{\mathrm{Var}(V)}{8(\mathrm{E}(V))^{3/2}}.$$

$\mathrm{Var}(V)$ has been determined by Swishchuk [24] to be

$$\begin{aligned}\mathrm{Var}(V) = \frac{\gamma^2 e^{-2kT}}{2k^3T^2}[&(2e^{2kT} - 4e^{kT}kT - 2)(\sigma_0^2 - \theta_0^2) \\ &+ (2e^{2kT}kT - 3e^{2kT} + 4e^{kT} - 1)\theta^2].\end{aligned} \tag{2.6}$$

and $\mathrm{E}(V)$ has already been determined in section 2.3. After applying this formula in Excel, we arrive at an approximation for the volatility swap fair strike for natural gas and crude oil:

$$\mathrm{E}(\sqrt{V_{NG}}) \approx 0.059567197,$$

$$\mathrm{E}(\sqrt{V_{oil}}) \approx 0.090925694.$$

Contract	Continuous	Discrete
NG Variance Swap Fair Strike	0.037183586	0.181172306
Crude Oil Variance Swap Fair Strike	0.011433191	0.114034599
NG Volatility Swap Fair Strike	0.059567197	0.425643403
Crude Oil Volatility Swap Fair Strike	0.090925694	0.337690093
NG/Crude Oil Covariance Swap	-	0.022832512
NG/Crude Oil Correlation Swap	-	0.158850823

Table 2.2: The variance, volatility, covariance, and correlation swap fair strike prices for natural gas and crude oil futures in continuous and discrete regimes following the Heston Model based on a 2019 dataset. Note that the discrete cases are realized values and are not calculated from the expected value of the realized values, i.e. the discrete calculations are empirical and the continuous are projections.

2.5 Summary of Calculations

The swap calculations are summarized in Table 2.2. No swap strike is very close to its discrete realized counterpart. The continuous setting should be more precise than the discrete setting when handling small datasets, but the exact point at which the discrete approach outperforms the continuous approach is unknown. Consider the average value of the crude oil volatility index (OVX) from section 4.5 of 0.338385, which matches the realized crude oil discrete volatility up to nearly 3 significant figures. The comparatively high performance of the discrete regime is likely because the continuous regime is making predictions whereas the discrete regime is simply summarizing the data. The discrete regime may be outperforming the continuous regime due to it having many observations (high n) which allow it to converge close to the correct value. Since the average value of the OVX is also essentially a summary of the data, it follows that the discrete crude oil volatility swap fair strike and the OVX should be very close. It is also worth noting that the maximum likelihood calibration is being done on the parameters from a mean-reverting model (namely the CIR

stochastic volatilities). In mean-reverting models, the parameters are very intimately connected and certain values for some parameters can throw off the maximum likelihood estimation for other parameters. For example, consider a mean-reverting process with extremely high volatility and extremely low speed of mean reversion. This process would have its mean reversion overpowered by the volatility, as such, the maximum likelihood calibration would have large errors associated with the mean reversion speed.

Chapter 3

Tests for mean reversion of oil and natural gas futures

3.1 ADF and PP Tests

Since the calculations in this paper depend on the Heston model. It will be valuable to verify the basic assumptions of this model. Specifically, it should be verified that the futures prices follow geometric Brownian motion and their volatility follows the mean-reverting CIR model.
To test the 2018 and 2019 datasets for mean-reverting prices, we will conduct two tests:

1. Augmented Dickey-Fuller (ADF) Test,
2. Phillips-Perron (PP) Test.

Fortunately, there is a MATLAB package that allows us to conduct these tests without needing to program them manually (see Appendix 8). Although only one test is necessary to assess mean reversion, it will be a good exercise to conduct both. For extra measure, the tests will be conducted twice for each of the 2018 and 2019 datasets, once on the futures prices,

and once on the log of the futures prices. The results are summarized in Table 3.1.

	Standard Futures Prices				Log Futures Prices			
Test	ADF Test		PP Test		ADF Test		PP Test	
Year	2018	2019	2018	2019	2018	2019	2018	2019
Crude Oil P-Value	0.3638	0.8336	0.3638	0.8336	0.3220	0.8755	0.3220	0.8755
Natural Gas P-Value	0.5170	0.3215	0.5170	0.3215	0.5410	0.3058	0.5410	0.3058

Table 3.1: Augmented Dickey-Fuller and Phillips-Perron tests conducted on one year of daily 2018 and 2019 crude oil and natural gas front month futures contracts.

Strangely, the ADF and PP tests yield the same p-values for the same data. Regardless, the tests indicate a failure to reject the null hypotheses of the two tests at any reasonable significance with p-values between 0.3 and 0.88. Therefore there is insufficient evidence to suggest that the oil and gas front month futures closing prices in 2018 and 2019 are mean-reverting. We will see in section 3.2 that performing a simple mean-reverting trading strategy on this dataset results in large returns but when following a momentum-based strategy, there are strongly negative returns. There is a significant possibility that the number of observations is insufficient to fully satisfy the ADF and PP tests despite the data potentially being mean-reverting. Plotting the time series of the data, (section 3.3) we see both the crude oil and the natural gas do not appear to exhibit strong mean-reversion behaviour but do have regions of strong volatility clustering. We distinguish two potential models to model this behaviour, geometric Brownian motion (GBM) and the Vasicek model. This is because GBM captures the random walk behaviour of the price processes, but does not enable volatility clustering on its own. It may be possible to fit the Vasicek process to the data such that its mean reversion simulates the volatility clustering at the expense of fitting the price process well. Additional tests

will be carried out to determine if the data reasonably follows either of these models; however, it is worth noting that GBM assumes positive prices. As seen in the 2020 WTI crude oil futures, the prices may occasionally become negative (see [23]). This is sufficient reason to question the validity of the use of GBM in the prices of these contracts. By contrast, the Vasicek model does not assume strictly positive prices. For this reason, the Vasicek model—as simple as it is—should be tested for its ability to model the prices of crude oil and natural gas futures. There is also the Ho-Lee model which models the mean as a deterministic function of time rather than a constant which may be worth considering in another paper. Time series plots of the data sets in section 3.3 indicate there may be a slight linear drift upwards or downwards in a given year but these drifts are very small. Specifically, we can see from the time series plot of the crude oil prices (Figure 3.8) that there could potentially be a mean-reverting level which changes in the two years from a linear upwards trend beginning at \$60 in the early two-thirds of 2018, to a flat linear trend in the latter half of 2019 hovering at \$50. The deterministic function of time in the Ho-Lee model could be defined such that it creates a moving mean-reverting level which approximately follows the price process. This is left as a passing remark as it exceeds the scope of this paper. Schwartz has previously proposed a one-factor model in which the log of the price process follows the Vasicek model, as well as similar more sophisticated two and three-factor models in [21] which factor in stochastic convenience yields and interest rates. There have not been any significant attempts at a modification of the Heston two-factor model in which the price process follows the Ho-Lee model or the Vasicek model that we are aware of. Since the Heston model uses GBM as its price process, it is vulnerable to negative prices. This makes a strong case for replacing the price process in the Heston model with a model that supports negative prices. The complexity given by CIR stochastic volatilities creates room for exceptionally obtuse expressions even using the simple GBM price

process, as is shown in chapter 5. This is likely a contributor to the lack of development of Heston variant models. Alternatively, variants on the Heston model may simply not be useful in financial markets.

We can assess the mean-reversion of the volatilities of crude oil and natural gas using the same tests as the spot prices but on volatility indices such as the OVX. Repeating the same approach as with the spot prices on the crude oil volatility index (ticker: OVX) for 2019, we see a p-value of 0.1071, which is still a failure to reject the null hypothesis at a significance of 5%, but consider that three years of VIX data (2017–2019) with the ADF test applied yields a p-value of 0.1708. The VIX is a well-known example of mean-reverting time series data, and the p-value of the OVX is significantly lower than it. Thus, we have an indication that the OVX was mean-reverting in this time period. Accepting this small leap in logic, it follows that the variance process of 2019 crude oil prices is also mean-reverting. The assessment of natural gas volatilities is significantly harder since there does not—as the writing of this paper—exist a natural gas equivalent of the OVX. Ding in 2021 derived a natural gas analogue to the OVX which they dubbed the NGVX. In their paper, they performed the ADF test on their derived NGVX data and found a unit root was present, indicating that natural gas volatilities were indeed mean-reverting in 2019 [8].

The use of the CIR model over say, the Vasicek model for the volatility process is characterized by the *smile* behaviour of the implied volatilities. This *smile* behaviour is defined by larger jumps in volatility when prices are far away from a contract's strike. Volatility indices are frequently reframed as measures of 'fear' in a given market and this *smile* behaviour appears to support that perspective. The CIR model's stochastic term contains the square root of the price which gives it this behaviour. This behaviour is not seen in the Vasicek model nor the continuous-time GARCH model.

For the CIR model to maintain strictly positive values, it must satisfy

$$\theta \geq \frac{\gamma^2}{2k} \tag{3.1}$$

called the *Feller condition* where θ is the mean-reverting level, γ is the volatility of the volatility and k is the mean reversion speed. Let σ_t^2 be a CIR process. If we define the stopping time $\tau_0 = \inf\{t \geq 0 : \sigma_t^2 = 0\}$, then when the Feller condition is satisfied, $\mathbb{P}(\tau_0 < \infty) = 0$. Since we have estimated θ, γ and k, we can assess to see if this condition is met in practice. For the 2019 crude oil dataset in the continuous setting, we know that $\theta = 0.1160$ and the corresponding $\gamma = 11.1293$ and $k = 174.4428$. Thus we have

$$\theta = 0.1140 \geq \frac{1.049^2}{2 * 7.951} = 0.06920 = \frac{\gamma^2}{2k}.$$

Similarly for the 2019 natural gas dataset following continuous-time,

$$\theta = 0.2069 < \frac{3.870^2}{2 * 7.493} = 0.9994 = \frac{\gamma^2}{2k}.$$

In the case of natural gas, the inequality is violated by a large margin. Evidently, this inequality does not need to be held in the real world. As it approaches 0, the CIR process given by

$$d\sigma_t^2 = k(\theta^2 - \sigma_t^2)dt + \gamma\sigma_t dw_t^2$$

becomes

$$d\sigma_t^2 = k\theta^2 dt$$

which will force the values to begin increasing again. Thus meeting the Feller condition is not of practical concern. It is important to note that failure to satisfy this condition when simulating the CIR process may result in complex values arising, this can be somewhat mitigated by only taking the real component of the process, but is far from desirable. This is interesting and it certainly motivates further discussion. This however extends beyond the scope of this paper and is left as another passing remark.

3.2 Mean-Reverting Algorithmic Trading Strategy

The Augmented Dickey-Fuller and Phillips-Perron tests indicate insufficient evidence to suggest that the 2018 and 2019 crude oil and natural gas futures are mean-reverting. These tests also may not have enough data to be fully satisfied and so an alternate approach is given in this section.

An asset price process with perfect guaranteed mean-reverting behaviour carries with it a simple trading strategy that results in significant returns when performed correctly. This approach is given in [12]. The trading strategy relies on comparing the long-run mean of a process with its current price. Knowing that this process is mean-reverting gives us information on its potential future movements. For example, if the long-run mean of a mean-reverting asset price process is \$100 and the current spot price is \$200, then the asset will feel a significant force pulling it downwards towards its mean. This would also be the case if the spot price was significantly less than the long-run mean, say \$50. An investor who recognizes this behaviour could buy a share of the asset at \$50 and sell once the process reaches its long-run mean of \$100, leaving a \$50 profit, excusing transaction costs. If the spot price goes over the mean, then he could short a share of the asset and close his position once the process reaches its mean. To generalize, the investor should enter a long position when the spot price is significantly below the long-run mean, and the investor should enter a short position when the spot price is significantly above the long-run mean. If the process is neither mean-reverting nor momentum-based, then we should expect random walk behaviour resulting in approximately neutral returns. If the process is not mean-reverting and instead momentum-based, then we should expect this strategy to fail dramatically, as the corresponding momentum-based strategy is exactly opposite to the mean-reverting one. The investor should be short when the spot price is below the long-run

mean and enter a long position when the spot price is above the long-run mean. Therefore we can apply this strategy to the 2018 and 2019 data sets for natural gas and crude oil: If they yield significantly positive returns while following a mean-reverting strategy then this would indicate that the forward prices of these commodities follow a mean-reverting pattern significantly more often than a momentum-based pattern.
This strategy requires three points to execute effectively:

- A way to determine the long-run mean or the mean-reverting level,
- The spot prices of the asset in question,
- A distance threshold to determine when to buy and sell the asset shares.

The spot price of the asset is public knowledge, and so only the first and last items are needed to execute this strategy. There are sophisticated ways to model an asset price process and determine its mean-reverting level such as in section 2.3. Since the mean-reversion of the 2018 and 2019 crude oil and natural gas prices are in question, a simple model-independent approach is taken using a 25-day simple moving average (SMA) for the mean-reverting level. The distance threshold is a topic of much discussion in [12] but since this specific algorithm is not going to be used for real market trading, a qualitative decision for the thresholds is enough, though a few different thresholds will be given for completeness. The MatLab code used to compute and plot the strategies is supplied in Appendix 8. The first panel is the distance of the spot price from the SMA, the thresholds are plotted as well. The second panel is the recommended investment decision by the algorithm: (+1) indicates a long position, (-1) indicates a short position and (0) indicates a neutral position in which all trades have been closed. The third panel plots the price process returns if the investor has simply bought a share and held onto it, versus the cumulative returns of the trading strategy.

As a control, this approach will first be applied to what is likely considered the best example of a mean-reverting financial process, the CBOE Volatility Index (ticker: VIX) over 3 years, 2017–2019. Three sets of plots are given, one with relatively low thresholds and the other with relatively high thresholds. From these plots, we can clearly see that the returns of the VIX are affected by the thresholds, but no sensible choice of thresholds will result in negative returns when they otherwise would have had positive results. This is because a higher threshold results in 'missing out' on some opportunities but since investing in a higher deviation from the long-run mean results in a higher likelihood of positive returns, these missed opportunities will not damage the returns enough to cause losses unless the price process stops being mean-reverting. In Figure 3.3, the algorithm has been set to follow a momentum-based strategy.

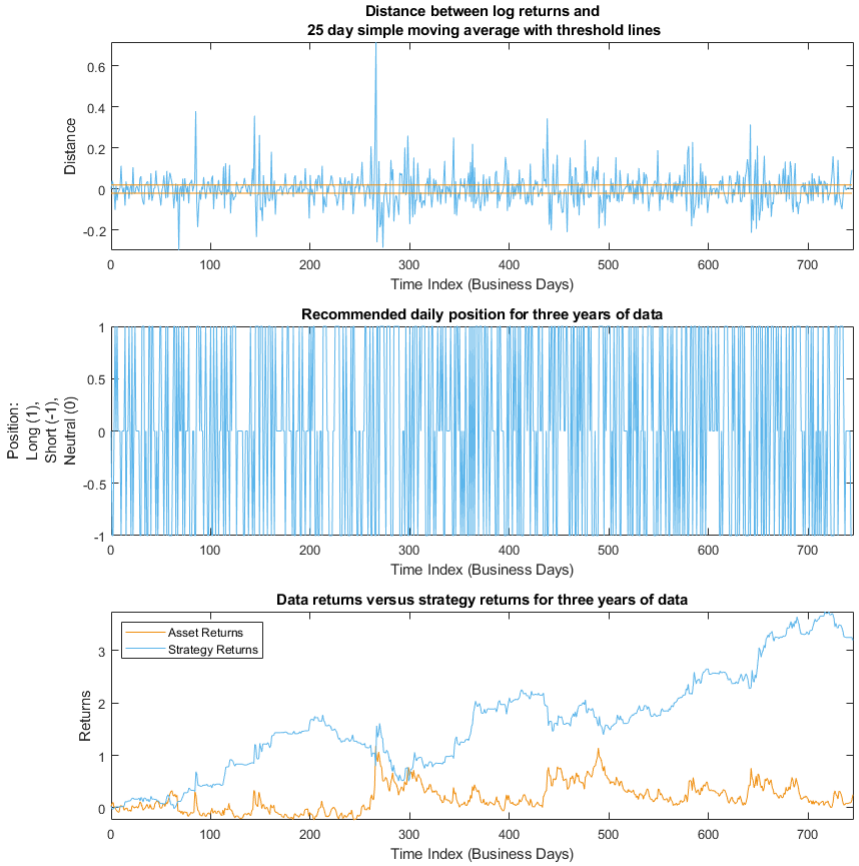

Figure 3.1: Three years of VIX data (2017–2019) with a mean-reverting trading strategy. The threshold level is set to be very low at 0.01.

As is evidenced by Figures 3.1, 3.2, and 3.3, this simple strategy will yield high returns on a mean-reverting dataset and catastrophic losses on a momentum-based dataset. Threshold lines have a clear effect on returns but setting them too high will not result in negative returns when they otherwise would be positive. Threshold lines set too low will prompt an investment when there is not a significant opportunity present, but will also never miss a good investment opportunity. Thus as long as the threshold lines

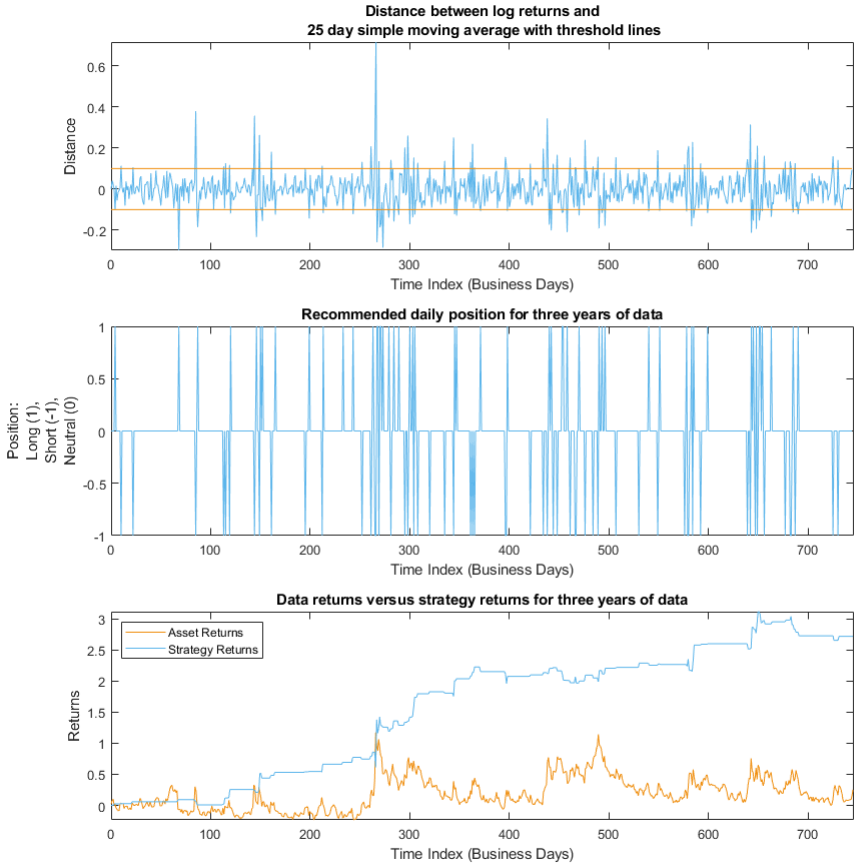

Figure 3.2: Three years of VIX data (2017–2019) with mean-reverting trading strategy. The threshold level is set to be reasonably high at 0.1.

are reasonably chosen the strategy appears to be an effective qualitative measure of the degree to which a price process may be mean-reverting.

Now we turn our attention to applying the algorithm to our 2018 and 2019 natural gas and crude oil data sets. If the algorithm yields positive returns then the data is likely to be more mean-reverting than momentum-based. The 2018 and 2019 natural gas data sets are in Figures 3.4 and 3.5. Figures 3.6 and 3.7 are for the 2018 and 2019 crude oil data sets.

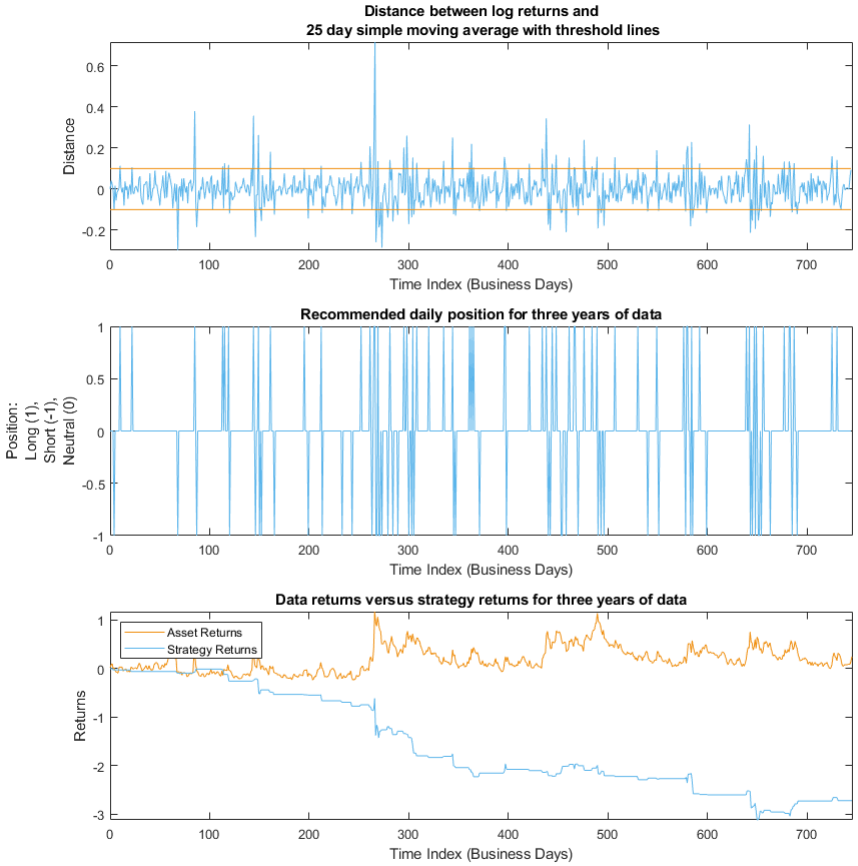

Figure 3.3: Three years of VIX data (2017–2019) with momentum-based trading strategy. The threshold level is set to be reasonably high at 0.1.

The returns for the 2018 natural gas, 2018 crude oil, and 2019 crude oil data sets (Figures 3.4, 3.6, and 3.7) each have positive returns varying from 20% to over 60%. These returns are not nearly as significant as with the VIX, but this is to be expected. It is clear these three data sets have some degree of mean-reversion in their behaviour but are far closer to random walks. The 2019 natural gas data is interesting as it starts with strongly positive returns but ends slightly negative. The negative returns

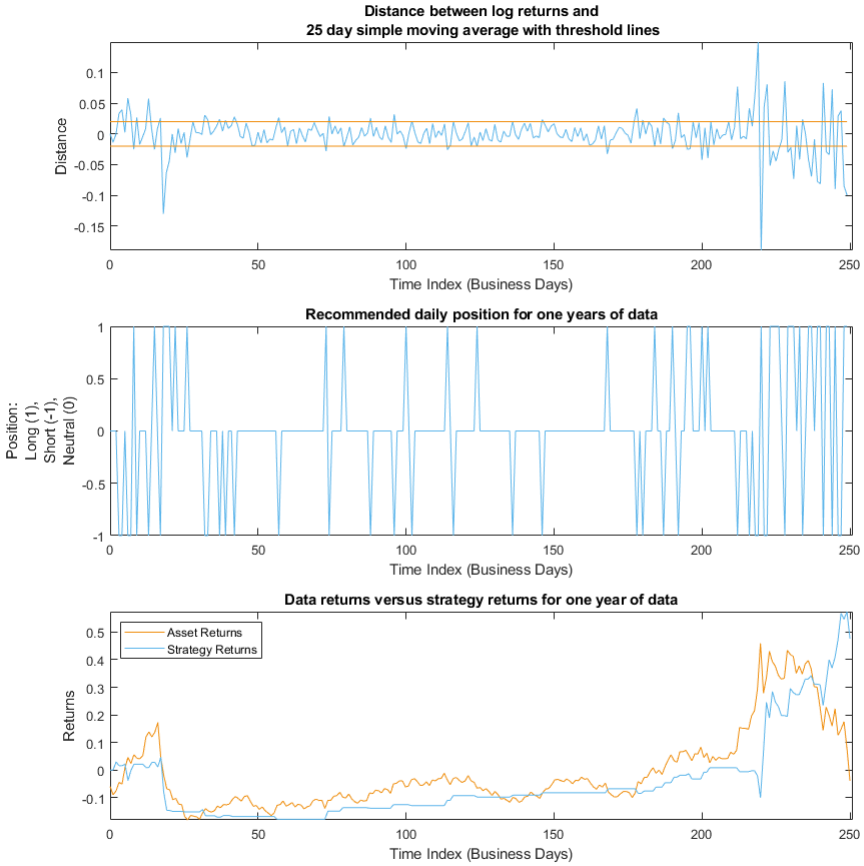

Figure 3.4: 2018 natural gas data applied to the mean-reversion trading algorithm. Threshold is qualitatively determined to be 0.02

are vanishingly small compared to the 300% negative returns of using the incorrect model on the VIX. Barring any coincidences, this suggests that in 2019, natural gas futures are somewhere between mean-reverting and momentum-based. In other words, it appears the 2019 natural gas futures prices were comparable to a random walk. Nonetheless, it seems the mean reversion of crude oil and natural gas prices has gotten weaker since the end of the 20^{th} century. This idea is strengthened in the results from the

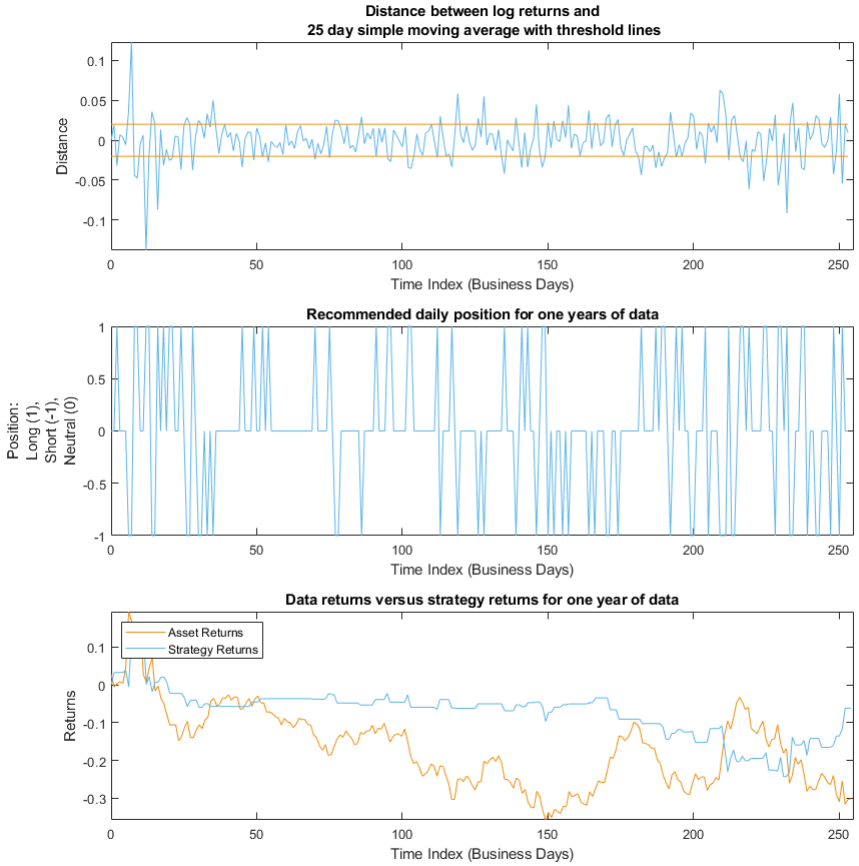

Figure 3.5: 2019 natural gas data applied to the mean-reversion trading algorithm. Threshold is qualitatively determined to be 0.02

ADF and PP tests from section 3.1.

Recall that the large p-values for the ADF and PP tests indicate a failure to reject the null hypothesis that the data is not mean-reverting (more specifically it indicates a failure to reject the null hypothesis that a unit root is not present, the presence of a unit root indicates mean-reverting behaviour). These commodity prices were mean-reverting in the 20^{th} century, but this trait has been fading over the past few decades. The

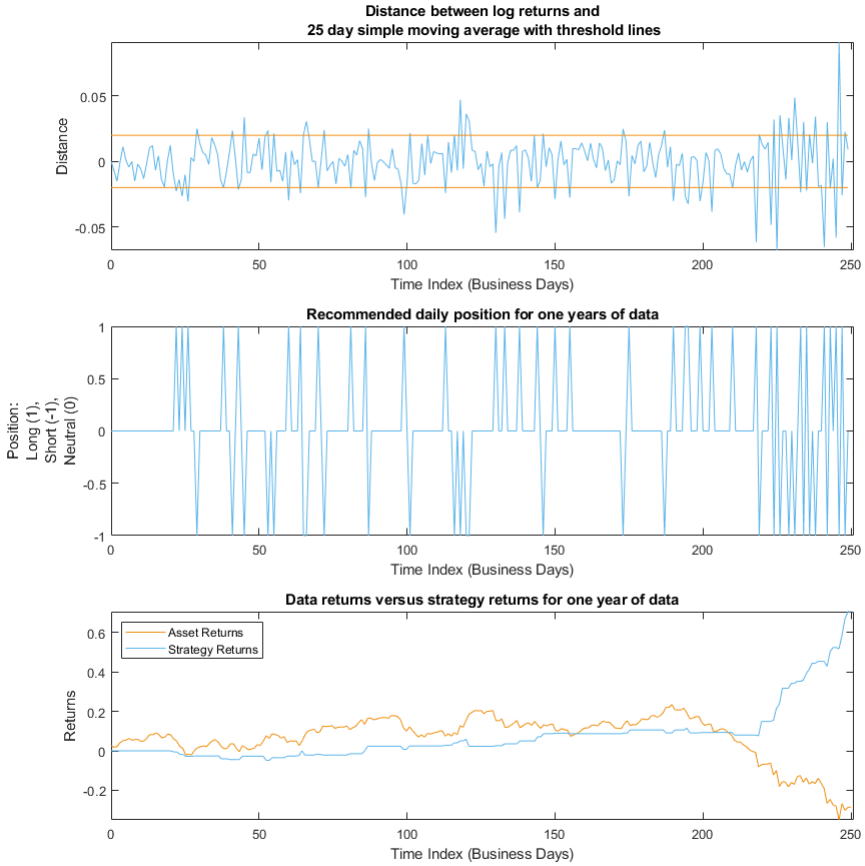

Figure 3.6: 2018 crude oil data applied to the mean-reversion trading algorithm. Threshold is qualitatively determined to be 0.02

phenomenon has been discussed in [10].

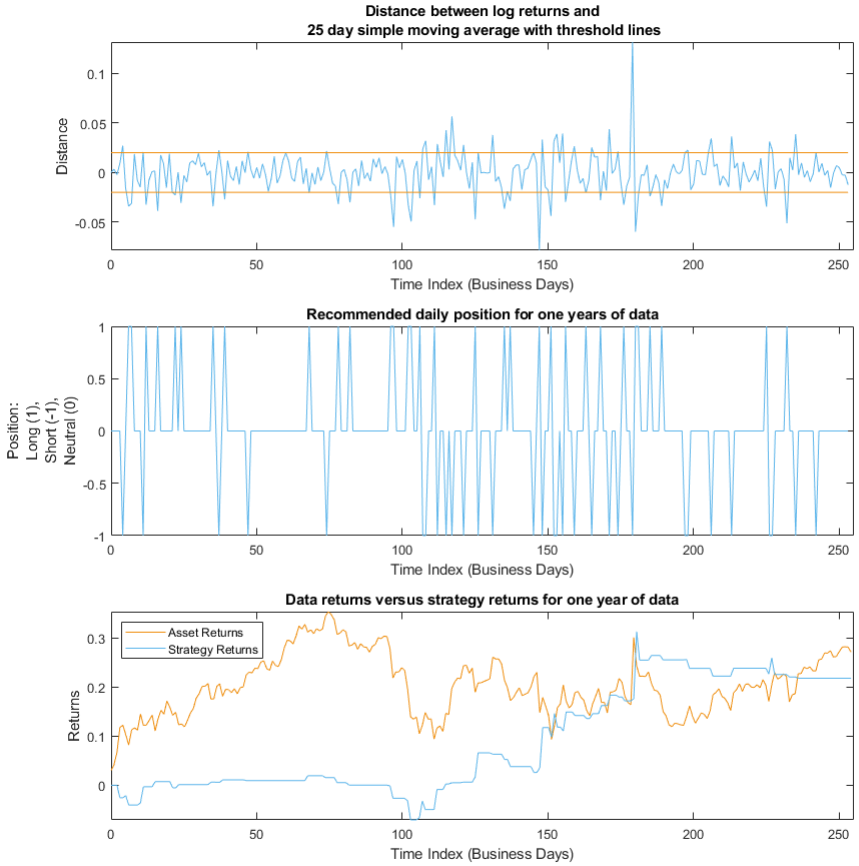

Figure 3.7: 2019 crude oil data applied to the mean-reversion trading algorithm. Threshold is qualitatively determined to be 0.02

3.3 Visual Assessment of Mean Reversion

The time series plots of the 2018 and 2019 natural gas and crude oil data sets are given in this section. Although a visual assessment is by no means an appropriate way to quantitatively model an asset price process, it is still a useful heuristic. Time series plots can be used to qualitatively assess if the asset price process exhibits volatility clustering or if it has strong mean-reverting properties. These observations can be used to strengthen

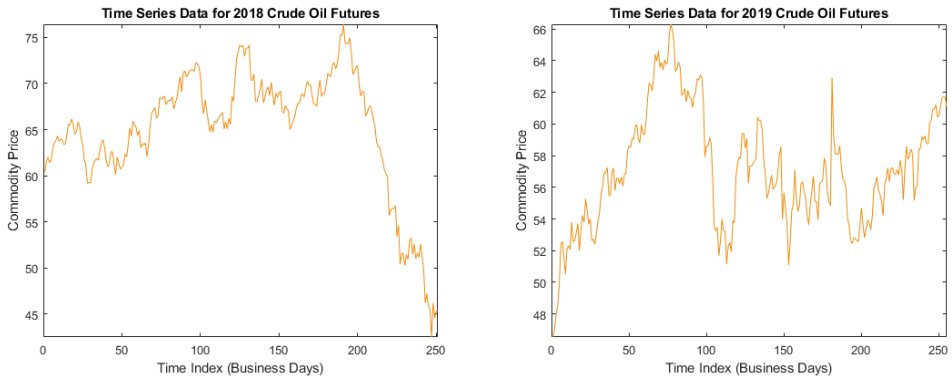

Figure 3.8: 2018 and 2019 front month crude oil futures close prices.

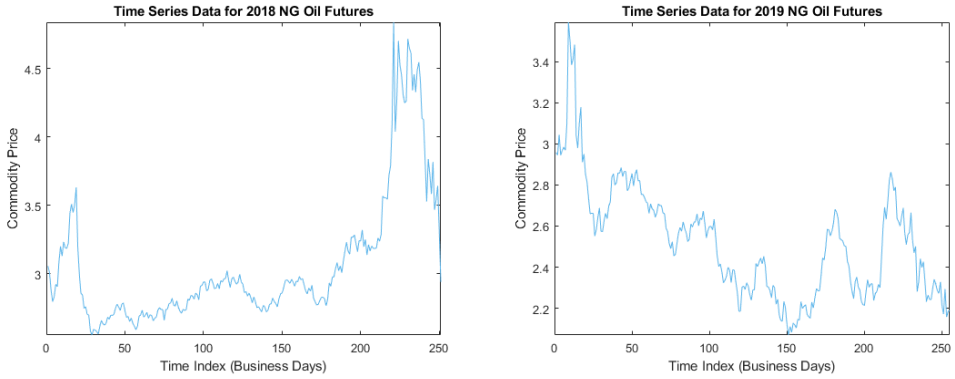

Figure 3.9: 2018 and 2019 front month natural gas futures close prices.

arguments about the properties of a process or inform decisions about possible viable models that can be used to fit the data. Figure 3.8 is the time series data for the crude oil futures and Figure 3.9 is the time series data for the natural gas futures. In the crude oil time series, it is apparent there is no clear mean reversion behaviour; the plots demonstrate more of a random walk behaviour. This idea is enforced by the meagre returns from the mean-reverting trading strategy. It is evident that the data exhibits significant volatility clustering since there are small intervals of time in which the prices of crude oil are relatively stable and also intervals in which the prices

are highly volatile. The Vasicek model and Schwartz's one-factor model do not account for volatility clustering as well as say, the Heston model. The two models are also mean-reverting which is not compelled strongly by the ADF and PP tests, nor the time series plots. Thus the Heston model should be a good fit for this data, as it can account for volatility clustering as well as non-mean-reverting price process behaviour.

The natural gas time series argument follows similar logic to the crude oil time series argument. Volatility clustering is obvious towards the end of 2018 and the start of 2019. In mid-2018 the process looks much more mean-reverting than crude oil. The mean-reverting trading strategy in both years does not return anywhere near the VIX in terms of returns and so in conjunction with the ADF and PP mean reversion tests, we conclude that natural gas futures were not strongly mean-reverting in 2018 and 2019. Thus the Heston model should be applicable for the natural gas time series as well.

Part II

Asset Model Comparisons

Introduction

This part is divided into 8 sections. In section 4.1 we determine the expected values, the variance, and the volatility of an asset following the Vasicek process defined under the risk-neutral measure Q for $i = 1, 2$ by

$$dS_t^i = a_i(b_i - S_t^i)dt + \sigma_i dw_t^i,$$

where $a > 0$, $b = b^* - \lambda\sigma/a$, $w_t^i := B_i(t) + \lambda t$, $B_i(t)$ is a standard brownian motion, and $\lambda \in \mathbb{R}$ is the market price of risk. In section 4.2 the results from the previous section are used to derive the covariance and correlation between two assets following the Vasicek model. Section 4.3 is a brief section devoted to the calibration of the Vasicek parameters, namely a_i, b_i, and σ_i for $i = 1, 2$. Section 4.4 applies the calibrated Vasicek model to our 2019 crude oil and natural gas by first determining the asset's realized variance, volatility, covariance, and correlation, then calculating the resulting values. In section 4.5, the crude oil volatility index (ticker: OVX) is used as a benchmark to assess the efficacy of the Vasicek model. Section 4.6 repeats the same process as the previous sections, but to the natural log of the data to get the Schwartz one-factor model. The resulting values are then compared against the crude oil volatility index to judge the effectiveness of the model. Section 4.7 is a digression into the Heston model defined under this risk-neutral measure Q for $i = 1, 2$ as

$$\begin{cases} \frac{dS_t^i}{S_t^i} = r_t^i dt + \sigma_t^i dw_t^i, & i = 1, 2, \\ d(\sigma_t^i)^2 = k_i(\theta_i^2 - (\sigma_t^i)^2)dt + \gamma_i \sigma_t^i dw_t^j, & j = i + 2. \end{cases}$$

With $k_i = k_i^* + \lambda_i$, $\theta_i^2 = k_i^* \theta_i^* / (k_i^* + \lambda_i)$, and $\lambda_i \in \mathbb{R}$ is the market price of risk. Finally, section 8 is a section devoted to explaining the separation of values between the continuous-time Heston model fair strike valuations and the discretely valued Heston realized variance, volatility, covariance, and correlation. The error distributions for k, θ, and γ are determined through simulation methods. These distributions are then used to loosely bound the range of errors of the parameters that may arise during calibration.

Chapter 4

Mean-Reverting Model Comparison

In this chapter, we perform the calculations required to derive the expected value, variance, covariance, and correlation between two Vasicek processes that are correlated. Next, the model is calibrated using least squares regression (LSR). Finally, numerical computations of the 2019 crude oil and natural gas data sets are applied to the results and the crude oil values are compared to the Crude Oil volatility index (ticker: OVX). Once the effectiveness of the Vasicek model is assessed, two other models will be compared with the OVX, the one-factor Schwartz model, and the Heston model.

The crude oil volatility index tracks the expected value of crude oil futures variances based on interpolating data from the United States Oil Fund (ticker: USO) and then square roots it to obtain the volatility. The OVX is expressed in percentage points.

Define the Vasicek process for $i = 1, 2$ in the risk-neutral setting as follows:

$$dS_t^i = a_i(b_i - S_t^i)dt + \sigma_i dw_t^i.$$

Where $a_i > 0$, $b_i = b_i^* - \lambda_i\sigma_i/a_i$, $w_t^i := B_i(t) + \lambda_i t$, $B_i(t)$ is a standard brownian motion, and $\lambda_i \in \mathbb{R}$ is the ith market price of risk. a_i is the speed

of mean reversion, b_i is the mean reversion level, S_t^i is the ith commodity price at time t, σ_i is the instantaneous volatility parameter, and w_t^i is the ith Brownian motion at time t. Moreover, let [–] be the quadratic variance, and assume that $d[w_t^1, w_t^2] = \rho dt$. Where ρ is the instantaneous correlation between the 2019 crude oil and 2019 natural gas datasets (calculated through the application of the CORREL() function in Excel to the dataset directly).

The solution to the Vasicek process is well-known and can be obtained by applying Ito's Lemma to the equation $f(x,t) = (x-b)e^{at}$. After minor simplification, we obtain:

$$S_t^i = S_0^i e^{-a_i t} + b_i(1 - e^{-a_i t}) + \sigma_i e^{-a_i t} \int_0^t e^{a_i s} dw_s^i.$$

Since w_s^i is a standard Brownian motion for all i, S_t^i is normally distributed. This fact is useful for the upcoming derivations.

4.1 Expected value, variance, and volatility of a Vasicek process

We begin with the expected value of the Vasicek process:

$$\mathrm{E}(S_t^i) = \mathrm{E}\left(S_0^i e^{-a_i t} + b_i(1 - e^{-a_i t}) + \sigma_i e^{-a_i t} \int_0^t e^{a_i s} dw_s^i \right).$$

By linearity of the expectation, the sum may be split. Since only the third term is nondeterministic the expectation of the first two terms is simply the terms themselves. Thus we arrive at

$$\mathrm{E}(S_t^i) = S_0^i e^{-a_i t} + b_i(1 - e^{-a_i t}) + \sigma_i e^{-a_i t}\, \mathrm{E}\left(\int_0^t e^{a_i s} dw_s^i \right).$$

The expected value of this Ito integral is 0. Therefore we arrive at the first results:

Theorem 4.1.1. *The expected value of a Vasicek process for $i = 1, 2$ is*

$$\mathrm{E}(S_t^i) = S_0^i e^{-a_i t} + b_i(1 - e^{-a_i t}).$$

Corollary 4.1.2. *The Vasicek process can be rewritten for $i = 1, 2$ as*

$$S_t^i = \mathrm{E}(S_t^i) + \sigma_i e^{-a_i t} \int_0^t e^{a_i s} dw_s^i.$$

The variance of the Vasicek process requires the calculation of the second moment of its stochastic element.

$$\mathrm{E}\left(\left(\sigma_i e^{-a_i t} \int_0^t e^{a_i s} dw_s^i\right)^2\right) = \sigma_i^2 e^{-2a_i t} \,\mathrm{E}\left(\left(\int_0^t e^{a_i s} dw_s^i\right)^2\right).$$

Applying Ito's isometry simplifies the integral:

$$\sigma_i^2 e^{-2a_i t} \,\mathrm{E}\left(\left(\int_0^t e^{a_i s} dw_s^i\right)^2\right) = \sigma_i^2 e^{-2a_i t} \,\mathrm{E}\left(\int_0^t e^{2a_i s} ds\right).$$

Now that the integral is deterministic, the expected value is trivial and all that remains is a simple integration,

$$\begin{aligned}
\sigma_i^2 e^{-2a_i t} \,\mathrm{E}\left(\int_0^t e^{2a_i s} ds\right) &= \sigma_i^2 e^{-2a_i t} \int_0^t \mathrm{E}(e^{2a_i s}) ds \\
&= \sigma_i^2 e^{-2a_i t} \int_0^t e^{2a_i s} ds \\
&= \sigma_i^2 e^{-2a_i t} \frac{1}{2a_i}(e^{2a_i t} - 1) \\
&= \frac{\sigma_i^2}{2a_i}(1 - e^{-2a_i t}).
\end{aligned}$$

The determination of the variance of the process is now simple since variances are translation invariant and the expected value of the Ito integral

vanishes to 0.

$$\begin{aligned}
\mathrm{Var}(S_t^i) &= \mathrm{Var}\left(S_0^i e^{-a_i t} + b_i(1-e^{-a_i t}) + \sigma_i e^{-a_i t}\int_0^t e^{a_i s} dw_s^i\right) \\
&= \mathrm{Var}\left(\sigma_i e^{-a_i t}\int_0^t e^{a_i s} dw_s^i\right) \\
&= \mathrm{E}\left(\left(\sigma_i e^{-a_i t}\int_0^t e^{a_i s} dw_s^i\right)^2\right) - \mathrm{E}^2\left(\sigma_i e^{-a_i t}\int_0^t e^{a_i s} dw_s^i\right) \\
&= \mathrm{E}\left(\left(\sigma_i e^{-a_i t}\int_0^t e^{a_i s} dw_s^i\right)^2\right) - 0 \\
&= \frac{\sigma_i^2}{2a_i}(1-e^{-2a_i t}).
\end{aligned}$$

The calculation of the volatility is simple now that the variance is obtained as $\mathrm{Vol}(S_t^i) := \sqrt{\mathrm{Var}(S_t^i)}$. Thus we have

$$\mathrm{Vol}(S_t^i) = \sigma_i\sqrt{\frac{(1-e^{-2a_i t})}{2a_i}}.$$

Hence we have proved

Theorem 4.1.3. *The variance and volatility of a Vasicek process for* $i = 1, 2$ *is*

$$\mathrm{Var}(S_t^i) = \frac{\sigma_i^2}{2a_i}(1-e^{-2a_i t}),$$

$$\mathrm{Vol}(S_t^i) = \sigma_i\sqrt{\frac{(1-e^{-2a_i t})}{2a_i}}.$$

4.2 Covariance and correlation of two correlated Vasicek processes

The calculation of the covariance between two correlated Vasicek processes is very similar to the calculation of their variances however, the application

of the Ito isometry is not as clear.

$$\mathrm{Cov}(S_t^1, S_t^2) = \mathrm{E}\{(S_t^1 - \mathrm{E}(S_t^1))(S_t^2 - \mathrm{E}(S_t^2))\}.$$

The expected values cancel with the expected values from the expanded expression for S_t^1 and S_t^2 (See Theorem 4.1.1):

$$\begin{aligned}
&\mathrm{E}\left((S_t^1 - \mathrm{E}(S_t^1))(S_t^2 - \mathrm{E}(S_t^2))\right) \\
&= \mathrm{E}\left\{ \left(\mathrm{E}(S_t^1) + \sigma_1 e^{-a_1 t}\int_0^t e^{a_1 s} dw_s^1 - \mathrm{E}(S_t^1)\right) \right. \\
&\qquad \left. * \left(\mathrm{E}(S_t^2) + \sigma_2 e^{-a_2 t}\int_0^t e^{a_2 s} dw_s^2 - \mathrm{E}(S_t^2)\right) \right\} \\
&= \mathrm{E}\left\{\sigma_1 e^{-a_1 t}\int_0^t e^{a_1 s} dw_s^1 \sigma_2 e^{-a_2 t}\int_0^t e^{a_2 s} dw_s^2\right\} \\
&= \sigma_1\sigma_2 e^{-(a_1+a_2)t}\,\mathrm{E}\left\{\int_0^t e^{a_1 s} dw_s^1 \int_0^t e^{a_2 s} dw_s^2\right\}.
\end{aligned}$$

Since $d[w_t^1, w_t^2] = \rho dt$, by Ito's isometry the expected value simplifies into

$$\mathrm{E}\left\{\int_0^t e^{a_1 s} dw_s^1 \int_0^t e^{a_2 s} dw_s^2\right\} = \rho\int_0^t e^{(a_1+a_2)s} ds.$$

Lastly, we can integrate and substitute this equation into the equation for the covariance between the two processes,

$$\begin{aligned}
&\sigma_1\sigma_2 e^{-(a_1+a_2)t}\,\mathrm{E}\left\{\int_0^t e^{a_1 s} dw_s^1 \int_0^t e^{a_2 s} dw_s^2\right\} \\
&\qquad = \sigma_1\sigma_2 e^{-(a_1+a_2)t}\rho\int_0^t e^{(a_1+a_2)s} ds \\
&\qquad = \frac{\rho\sigma_1\sigma_2(1 - e^{-(a_1+a_2)t})}{a_1 + a_2}.
\end{aligned}$$

The correlation between the processes is given by

$$\mathrm{Corr}(S_t^1, S_t^2) = \frac{\mathrm{Cov}(S_t^1, S_t^2)}{\mathrm{Vol}(S_t^1)\,\mathrm{Vol}(S_t^2)}.$$

Which proves the following theorem:

Theorem 4.2.1. *The covariance and correlation of two Vasicek processes is given by*

$$\mathrm{Cov}(S_t^1, S_t^2) = \frac{\rho\sigma_1\sigma_2}{a_1+a_2}(1-e^{-(a_1+a_2)t}),$$
$$\mathrm{Corr}(S_t^1, S_t^2) = \frac{2\rho\sqrt{a_1a_2}}{(a_1+a_2)}\frac{(1-e^{-(a_1+a_2)t})}{\sqrt{(1-e^{-a_1t})(1-e^{-a_2t})}}.$$

4.3 Calibration of the Vasicek process

The calibration of the Vasicek process is completed by using least squares regression (LSR) on a 1 year set of 2019 crude oil and natural gas futures. The regression line follows

$$S_{n+1} = \alpha S_i + \beta + \varepsilon$$

as outlined by Berg in [1]. The parameter values are determined using

$$a = -\frac{\ln\alpha}{\Delta t},$$
$$b = \frac{\beta}{1-\alpha},$$
$$\sigma = \mathrm{sd}(\varepsilon)\sqrt{\frac{-2\ln\alpha}{\Delta t(1-\alpha^2)}}.$$

Where $\Delta t = 1/252$ is the timestep of the data and $sd(\varepsilon)$ is the standard deviation of the error of the regression.

The determined parameters are included in Table 4.1. The instantaneous correlation, ρ, is determined to be -0.0812. The standard errors for the crude oil and natural gas αs are 0.0206 and 0.0166 respectively. The R^2 values for the crude oil and natural gas regressions are

$$R^2_{oil} = 0.891208551 \text{ and } R^2_{NG} = 0.930689987.$$

	Crude Oil	Natural Gas
α	0.9319	0.9628
β	3.9440	0.0909
Δt	0.0040	0.0040
$sd(\varepsilon)$	1.1751	0.0421
a	17.7861	9.5528
b	57.8758	2.4444
σ	19.3154	0.6802

Table 4.1: Vasicek model parameters for one year of daily 2019 crude oil and natural gas futures.

4.4 Application of the Vasicek process to crude oil and natural gas

Before we apply the datasets to the derived equations, we need to determine the realized variance, volatility, covariance, and correlation. These values are found by integrating over $[0, T]$ and dividing by T where T is the expiry time of the contract. This gives an average value of the function. Let $i = 1, 2$ then,

$$\begin{aligned}
\mathrm{Var}_R(S_T^i) &:= \frac{1}{T}\int_0^T \mathrm{Var}(S_s^i)ds, \\
\mathrm{Vol}_R(S_T^i) &:= \sqrt{\frac{1}{T}\int_0^T \mathrm{Var}(S_s^i)ds}, \\
\mathrm{Cov}_R(S_T^1, S_T^2) &:= \frac{1}{T}\int_0^T \mathrm{Cov}(S_s^1, S_s^2)ds, \\
\mathrm{Corr}_R(S_T^1, S_T^2) &:= \frac{\mathrm{Cov}_R(S_T^1, S_T^2)}{\mathrm{Vol}_R(S_T^1)\,\mathrm{Vol}_R(S_T^2)}.
\end{aligned}$$

Fortunately, these integrals require only simple integrations. We will

start with the realized variance.

$$\begin{aligned}
\mathrm{Var}_R(S_T^i) &= \frac{1}{T}\int_0^T \mathrm{Var}(S_s^i)ds, && (4.1)\\
&= \frac{1}{T}\frac{\sigma_i^2}{2a_i}\int_0^T (1-e^{-2a_i s})ds && (4.2)\\
&= \frac{1}{T}\frac{\sigma_i^2}{2a_i}\left(T - \frac{1}{2a_i}(-e^{-2a_i T}+1)\right) && (4.3)\\
&= \frac{1}{T}\frac{\sigma_i^2}{2a_i}\left(T + \frac{1}{2a_i}(e^{-2a_i T}-1)\right) && (4.4)\\
&= \frac{\sigma_i^2}{2a_i} + \frac{\sigma_i^2}{4a_i^2 T}(e^{-2a_i T}-1). && (4.5)
\end{aligned}$$

From this, the next theorem is immediately obtained.

Theorem 4.4.1. *The realized variance and volatility of a Vasicek process for $i = 1, 2$ is given by*

$$\mathrm{Var}_R(S_T^i) = \frac{\sigma_i^2}{2a_i} + \frac{\sigma_i^2}{4a_i^2 T}(e^{-2a_i T}-1),$$

$$\mathrm{Vol}_R(S_T^i) = \sqrt{\mathrm{Var}_R(S_T^i)}.$$

Now, we perform similar steps for the realized covariance and correlation.

$$\begin{aligned}
\mathrm{Cov}_R(S_T^1, S_T^2) &= \frac{1}{T}\int_0^T \mathrm{Cov}(S_s^1, S_s^2)ds && (4.6)\\
&= \frac{1}{T}\int_0^T \frac{\rho\sigma_1\sigma_2(1-e^{-(a_1+a_2)s})}{a_1+a_2}ds && (4.7)\\
&= \frac{1}{T}\frac{\rho\sigma_1\sigma_2}{a_1+a_2}\int_0^T (1-e^{-(a_1+a_2)s})ds && (4.8)\\
&= \frac{1}{T}\frac{\rho\sigma_1\sigma_2}{a_1+a_2}\left(T - \frac{1}{a_1+a_2}(-e^{-(a_1+a_2)T}+1)\right). && (4.9)
\end{aligned}$$

Notice the similarities between (4.4) and (4.9). Namely, if we set $\rho = 1$, $a_1 = a_2$, and $\sigma_1 = \sigma_2$ then (4.4) and (4.9) are exactly equal. This is a

useful check to ensure the work performed is correct. Naturally, the realized correlation is immediately obtained after minor simplification and we have proven the next theorem.

Theorem 4.4.2. *The realized covariance and correlation of two Vasicek processes correlated by ρ is given by*

$$\mathrm{Cov}_R(S_T^1, S_T^2) = \frac{\rho\sigma_1\sigma_2}{a_1+a_2} + \frac{\rho\sigma_1\sigma_2}{T(a_1+a_2)^2}(e^{-(a_1+a_2)T} - 1),$$

$$\begin{aligned}\mathrm{Corr}_R(S_T^1, S_T^2) &= \frac{\mathrm{Cov}_R(S_T^1, S_T^2)}{\mathrm{Vol}_R(S_T^1)\,\mathrm{Vol}_R(S_T^2)} \\ &= \rho\frac{\frac{1}{a_1+a_2} + \frac{e^{-(a_1+a_2)T}-1}{T(a_1+a_2)}}{\sqrt{\left(\frac{1}{2a_1} + \frac{e^{-2a_1T}-1}{4a_1^2T}\right)\left(\frac{1}{2a_2} + \frac{e^{-2a_2T}-1}{4a_2^2T}\right)}}.\end{aligned}$$

A Vasicek price process for commodity prices by itself is not a stochastic volatility model; any practical discussion about the fair strike price of swaps on variance, volatility, covariance, and correlation in this model is nonsensical. To compare these prices to the volatility index (OVX) however, we must treat them as we would any practical swap. Now that we have the needed theorems we can apply Theorems 4.4.1 and 4.4.2 to the 2019 datasets and obtain relevant values to compare to the OVX. Inputting the equations from Theorems 4.4.1 and 4.4.2 into Microsoft Excel the following table is obtained. As can be seen from the table, the correlation and covariance between the natural gas and crude oil futures appear to be very weakly correlated, but this makes sense since the R^2 values are so high. Most of the price of these commodities is determined by the previous day, overshadowing the effects of correlation. The volatility of crude oil is higher than that of natural gas which is consistent with the time series plots of the data. The realized correlation (as defined above) is very similar to the instantaneous correlation (calculated using the Excel function CORREL() on the dataset.), $\rho = -0.0812$.

	Crude Oil	Natural Gas
Variance	10.1933	0.0230
Volatility	3.1927	0.1515
Covariance	-0.0376	-0.0376
Correlation	-0.0777	-0.0777

Table 4.2: Vasicek model variance, volatility, covariance, and correlation for one year of daily 2019 crude oil and natural gas front month futures closing prices, $T = 1$.

4.5 Comparison between Vasicek model and the crude oil volatility index

The Crude Oil Volatility Index (OVX) data from 2019 is summarized below. Unfortunately, we do not know of a similar index for natural gas, nor the correlation or covariance between them. There are indices from the CBOE for the implied correlation for SPX with rotating tickers $ICJ, $KCJ, and $JCJ which cycle based on the maturity dates of the contracts. There is also an implied correlation index with ticker COR3M. None of these indices are useful for this paper as they are implied correlations and are not focused on commodities in the energy sector.

	Crude Oil Volatility Index (% points) (OVX)	Crude Oil Volatility Index (OVX)
High	54.7200	0.5472
Low	24	0.24
Average	33.8385	0.3384
Median	33.4000	0.3340

Table 4.3: A summary of 2019 OVX data. The first column is the values as given in the data, the second is the values divided by 100 to take them out of percent terms for easier reference.

In Table 4.3 it can be seen that the median and average values are close. with a high of nearly 55% and a low of 24%. These values are substantially

different from the volatility given by the Vasicek model. This indicates that the Vasicek model is likely not sufficient to model the price processes of crude oil.

4.6 Comparison between the Schwartz one-factor model and the crude oil volatility index

In [21] Schwartz's first proposed model is the Vasicek model but with the stochastic prices equal to $\ln(S_t^i)$ instead of S_t^i. In his paper, the crude oil prices are modelled well by this process. We will follow Schwartz's approach and apply the same analysis as in section 4.4 but to the log prices instead. Calibrating the model yields Table 4.4 and applying the calculations yields Table 4.5. Again, the correlation is similar to ρ, but now the volatility of the crude oil is much closer to the observed OVX data from the same time period with a minimum of 24%. This supports Schwartz's evidence that the crude oil price process follows his proposed process somewhat well, but is still very far off from the average of 33%.

	Crude Oil	Natural Gas
α	0.9285	0.9663
β	0.2901	0.0298
Δt	0.0040	0.0040
$sd(\varepsilon)$	0.0820	0.0147
a	18.6995	8.6320
b	4.0564	0.8858
σ	1.3495	0.2372

Table 4.4: Schwartz one-factor model parameters for daily 2019 crude oil and natural gas futures.

	Crude Oil	Natural Gas
Variance	0.0474	0.0031
Volatility	0.2177	0.0554
Covariance	-0.0007	-0.0007
Correlation	-0.0587	-0.0587

Table 4.5: Schwartz one-factor model variance, volatility, covariance, and correlation for one year of daily 2019 crude oil and natural gas front month futures closing prices, $T = 1$, $\rho = -0.0627$.

4.7 Comparison between the Heston model and the crude oil volatility index

In [24] Swishchuk derives closed-form solutions for variance and volatility swaps in the Heston model using a change of time approach. These calculations can be compared to the crude oil volatility index as well. Table 4.6 summarizes the values obtained from this model using the same data. Note that the GARCH(1,1) calibrations were performed using log-returns of the price data.

	Crude Oil	Natural Gas
Variance	0.0114	0.0372
Volatility	0.0909	0.0596

Table 4.6: Continuously realized variance and volatility of the log returns of the 2019 crude oil dataset following the Heston model.

As can be seen from Table 4.6, the volatility of the continuous-time realized volatility does not match the volatility observed by the crude oil volatility index. Note that the discrete volatility and variances have also been calculated (also using log-returns) and are given in Table 4.7. Here, the volatility is equal to the average of the OVX up to nearly 3 significant figures (OVX: 0.3384 versus Heston discrete: 0.3377).

	Crude Oil	Natural Gas
Variance	0.1140	0.1812
Volatility	0.3377	0.4256

Table 4.7: Discretely realized variance and volatility of the log returns of the 2019 crude oil dataset following the Heston model.

A possible reason for the large errors in Table 4.6 is the calibration method. Appendix 8 is devoted to this discussion.

Part III

Heston Model Continuous-Time Covariance and Correlation Swaps

Introduction

This part will be dedicated to the derivation of formulas for the continuous-time covariance and correlation swaps following the Heston model. First, several useful facts will be given in the form of lemmas. Next, the formula for the covariance swap will be determined. Finally, a formula for the correlation swap will be determined.

The model used will be the Heston stochastic volatility model under the risk-neutral measure Q,

$$\begin{cases} \frac{dS_t^i}{S_t^i} = r_t^i dt + \sigma_t^i dw_t^i, & i = 1, 2, \\ d(\sigma_t^i)^2 = k_i(\theta_i^2 - (\sigma_t^i)^2)dt + \gamma_i \sigma_t^i dw_t^j, & j = i + 2. \end{cases} \tag{4.10}$$

With $k_i = k_i^* + \lambda_i$, $\theta_i^2 = k_i^* \theta_i^* / (k_i^* + \lambda_i)$, and $\lambda_i \in \mathbb{R}$ is the ith market price of risk. Where S_t^i is the ith price process for a given asset, r_t^i is the ith risk-free rate, σ_t^i is the ith stochastic volatility, k_i is the ith constant speed of mean reversion, θ_i is the ith constant mean-reverting level, γ_i is the ith constant volatility of the volatility, w_t^1 and w_t^2 are standard Brownian motions with quadratic variance, $[w_t^1, w_t^2] = \rho_t$, and w_t^3 and w_t^4 are independent standard Brownian motions, and finally ρ_t is a deterministic function of time which may be constant. w_t^i and w_t^{i+2} are taken as independent in the interest of simplicity only. We note that additional volatility dynamics may be captured by correlating these two sets of Brownian motions but this would increase the complexity of the calculations in this part substantially. As seen in [23], futures prices may occasionally become negative. These are rare

and momentary occurrences but when they do happen the GBM process of the Heston model becomes invalid. As a result, for this case, one could use other models which accommodate negative prices as a stand-in for the Heston model such as the Vasicek model. A discussion about the feasibility of various models can be found in [23].

Powers of expected values of some stochastic process X_t will be written as

$$(\mathrm{E}(X_t))^n := \mathrm{E}^n(X_t),$$

and are with respect to the risk-neutral measure in the filtered probability space $(\Omega, \mathcal{F}_t, \mathbb{Q})$ where Ω is the sample space, $\mathcal{F}_t$ is the filtration with respect to the time, $t > 0$, and $\mathbb{Q}$ is the risk-neutral measure. Note that the n-th power of a Brownian motion will be written as $(w_t^i)^n$ since this avoids ambiguity about what is an index and what is an exponent. The subscript on w_t^i will be written as $w^i(t)$ when t is sufficiently complex to warrant more space.

Next, define $\Delta_i := (\sigma_0^i)^2 - \theta_i^2$ and $b_t^i := \tilde{w}^j((\phi_t^i)^{-1})$ where $i = 1, 2$ and $j = i+1$. The equations in the upcoming derivations become exceptionally long and complex, thus substitution is heavily relied upon for practical reasons, and to aid clarity. In fact, in the subsequent chapters, the expressions will become so long and complex that it is not practically feasible to write them explicitly on paper.

Chapter 5

Derivation of Continuous-Time Covariance and Correlation Swap Fair Strike Prices in the Heston Model

5.1 Preliminary Facts

These facts are mostly simple and well-known facts but are of essential use in the main results of this paper. They are given explicitly as lemmas now since as the expressions become progressively more complex, the logical steps in each proof become increasingly difficult to follow.

Lemma 5.1.1. *Let $0 \leq t \in \mathbb{R}$ and W_t be a standard Brownian motion. Then*

$$E\left\{(W_t)^n\right\} = \begin{cases} 0 & \text{if } n \text{ is odd,} \\ t^{n/2}(n-1)!! & \text{if } n \text{ is even,} \end{cases}$$

where $(n-1)!!$ *is the semifactorial function, i.e.*

$$(n-1)!! = \prod_{i=1}^{(n+1)/2} (2i-1) = (n-1)(n-3)\cdots(3)(1).$$

Lemma 5.1.2. *Let* $0 \leq t \in \mathbb{R}$ *and* w_t *be a standard Brownian motion. Then*

1. $\mathrm{E}(w_t) = 0$,
2. $\mathrm{E}((w_t)^2) = t$,
3. w_t *is normally distributed with mean* 0 *and variance* t.

Proof. The proof follows immediately from Lemma 5.1.1 with substitutions $n = 1, 2$ for each respective item. Item 3 is proved by items 1 and 2 together. □

Remark 5.1.3. Let X_t and Y_t be two independent stochastic processes. Then $\mathrm{E}(X_t Y_t) = \mathrm{E}(X_t)\,\mathrm{E}(Y_t)$.

Theorem 5.1.4 (Swishchuk [24])**.** *Let* σ_t^2 *be defined by 4.10. Then for* $i = 1, 2$ *and* $j = i + 1$,

$$(\sigma_t^i)^2 = e^{-k_i t}(\Delta_i + \tilde{W}^j((\phi_t^i)^{-1})) + \theta_i^2,$$

where $(\phi_t^i)^{-1}$ *is the inverse to*

$$\phi_t^i = \gamma_i^{-2} \int_0^t \{e^{k_i \phi_s^i}(\Delta_i + \tilde{W}_s^j + \theta_i^2 e^{2k_i\phi_s^i})\}^{-1} ds.$$

Theorem 5.1.5 (Brockhaus and Long [2])**.** *Let* X_t *be a stochastic process with* $t \geq 0$, *then* $\mathrm{E}(X_t)$ *can be approximated with*

$$\mathrm{E}\left(\sqrt{X_t^2}\right) \approx \sqrt{\mathrm{E}\,(X_t^2)} - \frac{\mathrm{Var}(X_t^2)}{8\,\mathrm{E}^{3/2}(X_t^2)}.$$

Theorem 5.1.5 is a clever application of a second-order Taylor series expansion of the function $f(x) = \sqrt{x}$ around the point $V_0 = X_t^2$. This approximation is given here because a similar derivation will be given in the next section for the bivariate case.

5.2 Covariance Swaps

The covariance swap will now be derived. We start with the previously derived expression for the fair strike of the contract with equation (1.2) since the fair strike of a swap is the most important value. It is simple to find the value of contracts at other strikes once the fair strike is determined.

$$K_{cov} = \mathrm{E}(\mathrm{Cov}_R(S^1, S^2)),$$

where

$$\mathrm{Cov}_R(S^1, S^2) := \frac{1}{T}\int_0^T \mathrm{Cov}(S^1, S^2)dt$$

is the realized covariance between assets S^1 and S^2. Swishchuk [24] has already shown that

$$\mathrm{E}(\mathrm{Cov}_R(S^1, S^2)) = \frac{1}{T}\int_0^T \rho_t \,\mathrm{E}(\sigma_t^1 \sigma_t^2)dt.$$

The ρ_t can be brought out of the expected value since it is modelled as a deterministic function of time. This quantity by itself is difficult to calculate, so we will rely on an approximation similar Brockhaus-Long approximation given by Theorem 5.1.5, but derived using the bivariate second-order Taylor approximation.

The second order bivariate taylor expansion of a function $f(x, y)$ about a point $a = [a_1, a_2]$ with $u = x - a_1$ and $v = y - a_2$ is given by

$$T_2(x, y) = f(a) + f_x(a)u + f_y(a)v + f_{xx}(a)\frac{u^2}{2} + f_{yy}(a)\frac{v^2}{2} + f_{xy}(a)uv.$$

Next we substitute in $f(x, y) = \sqrt{xy}$ and $a = [\mathrm{E}((\sigma_t^1)^2), \mathrm{E}((\sigma_t^2)^2)]$. We have several partial derivatives to find, and some simplifications we can make afterwards. Observe that

$$
\begin{aligned}
f(x,y) &= \sqrt{xy}, & f(a) &= \sqrt{a_1 a_2} \\
f_x(x,y) &= \tfrac{y}{2\sqrt{xy}} = \tfrac{1}{2}\sqrt{\tfrac{y}{x}}, & f_x(a) &= \tfrac{1}{2}\sqrt{\tfrac{a_2}{a_1}} \\
f_y(x,y) &= \tfrac{x}{2\sqrt{xy}} = \tfrac{1}{2}\sqrt{\tfrac{x}{y}}, & f_y(a) &= \tfrac{1}{2}\sqrt{\tfrac{a_1}{a_2}} \\
f_{xx}(x,y) &= \tfrac{-y^2}{4\sqrt{(xy)^3}} = -\tfrac{1}{4}\sqrt{\tfrac{y}{x^3}}, & f_{xx}(a) &= -\tfrac{1}{4}\sqrt{\tfrac{a_2}{a_1^3}} \\
f_{yy}(x,y) &= \tfrac{-x^2}{4\sqrt{(xy)^3}} = -\tfrac{1}{4}\sqrt{\tfrac{x}{y^3}}, & f_{yy}(a) &= -\tfrac{1}{4}\sqrt{\tfrac{a_1}{a_2^3}} \\
f_{xy}(x,y) &= \tfrac{1}{4\sqrt{xy}}, & f_{xy}(a) &= \tfrac{1}{4\sqrt{a_1 a_2}}
\end{aligned}
$$

gives us the Taylor coefficients. Thus the Taylor approximation becomes

$$
T_2(x,y) = \sqrt{a_1 a_2} + \frac{1}{2}\sqrt{\frac{a_2}{a_1}}u + \frac{1}{2}\sqrt{\frac{a_1}{a_2}}v - \frac{1}{4}\sqrt{\frac{a_2}{a_1^3}}\frac{u^2}{2} - \frac{1}{4}\sqrt{\frac{a_1}{a_2^3}}\frac{v^2}{2} + \frac{1}{4\sqrt{a_1 a_2}}uv.
$$

Now, substituting in $x = \sigma_t^1$ and $y = \sigma_t^2$ and taking the expectation of both sides, a few things will happen. Firstly, terms 1 and 2 will become zero since

$$
\mathrm{E}(u) = \mathrm{E}(x - a_1) = \mathrm{E}((\sigma_t^1)^2) - \mathrm{E}((\sigma_t^1)^2) = 0
$$

and

$$
\mathrm{E}(v) = \mathrm{E}(y - a_2) = \mathrm{E}((\sigma_t^2)^2) - \mathrm{E}((\sigma_t^2)^2) = 0.
$$

Term 5 will also be zero since by assumption, $\mathrm{Cov}((\sigma_t^1)^2, (\sigma_t^2)^2) = \mathrm{E}(uv) = 0$ from their respective independent Brownian motions. Thus we are left with

$$
\mathrm{E}\left(\sqrt{(\sigma_t^1\sigma_t^2)^2}\right) \approx \sqrt{a_1 a_2} - \frac{1}{8}\sqrt{\frac{a_2}{a_1^3}}\,\mathrm{E}(u^2) - \frac{1}{8}\sqrt{\frac{a_1}{a_2^3}}\,\mathrm{E}(v^2).
$$

But $\mathrm{E}(u^2) = \mathrm{Var}((\sigma_t^1)^2)$ and $\mathrm{E}(v^2) = \mathrm{Var}((\sigma_t^2)^2)$. Substituting everything in our approximation becomes

$$
\begin{aligned}
\mathrm{E}\left(\sqrt{(\sigma_t^1\sigma_t^2)^2}\right) \approx & \sqrt{\mathrm{E}((\sigma_t^1)^2)\,\mathrm{E}((\sigma_t^2)^2)} - \frac{1}{8}\sqrt{\frac{\mathrm{E}((\sigma_t^2)^2)}{\mathrm{E}^3((\sigma_t^1)^2)}}\,\mathrm{Var}((\sigma_t^1)^2) \\
& - \frac{1}{8}\sqrt{\frac{\mathrm{E}((\sigma_t^1)^2)}{\mathrm{E}^3((\sigma_t^2)^2)}}\,\mathrm{Var}((\sigma_t^2)^2). \qquad (5.1)
\end{aligned}
$$

Since $\mathrm{E}(\sigma_t^1\sigma_t^2)$ may be written as $\mathrm{E}(\sqrt{(\sigma_t^1\sigma_t^2)^2})$, our approximation may be used to value the covariance swap. Substituting this in to our expression for $\mathrm{E}(\mathrm{Cov}_R(S^1, S^2))$ we have

$$\begin{aligned}&\mathrm{E}(\mathrm{Cov}_R(S^1, S^2)) \approx \\ &\frac{\rho_t}{T}\int_0^T \sqrt{\mathrm{E}((\sigma_t^1)^2)\,\mathrm{E}((\sigma_t^2)^2)} - \frac{1}{8}\sqrt{\frac{\mathrm{E}((\sigma_t^2)^2)}{\mathrm{E}^3((\sigma_t^1)^2)}}\,\mathrm{Var}((\sigma_t^1)^2) \\ &\qquad - \frac{1}{8}\sqrt{\frac{\mathrm{E}((\sigma_t^1)^2)}{\mathrm{E}^3((\sigma_t^2)^2)}}\,\mathrm{Var}((\sigma_t^1)^2)dt.\end{aligned} \tag{5.2}$$

Thus the problem reduces to the evaluation of $\mathrm{E}((\sigma_t^1\sigma_t^2)^2)$ and $\mathrm{Var}((\sigma_t^i)^2)$ for $i = 1, 2$, but $\mathrm{Var}((\sigma_t^i)^2) = \mathrm{E}((\sigma_t^i)^4) - \mathrm{E}^2((\sigma_t^i)^2)$. Therefore only $\mathrm{E}((\sigma_t^i)^4)$ and $\mathrm{E}((\sigma_t^i)^2)$ need to be found.

Beginning with $\mathrm{E}((\sigma_t^1\sigma_t^2)^2)$, recall that $(\sigma_t^i)^2, i = 1, 2$ is given in Theorem 5.1.4 as a function of multiple constants, time, and a single stochastic element, $\tilde{W}^j((\phi_t^i)^{-1})$ where $j = i+1$. Since $\tilde{W}_t^j$ is directly derived from W_t^j (see Ikeda and Wanatabe [14]) it immediately follows that $(\sigma_t^1)^2$ is independent from $(\sigma_t^2)^2$ and remark 5.1.3 applies. We have

$$\mathrm{E}((\sigma_t^1\sigma_t^2)^2) = \mathrm{E}((\sigma_t^1)^2)\,\mathrm{E}((\sigma_t^2)^2)$$

where each of these expectations is given by Swishchuk [24] as

$$\mathrm{E}((\sigma_t^i)^2) = e^{-k_i t}\Delta_i + \theta_i^2,$$

where $\Delta_i = (\sigma_0^i)^2 - \theta_i^2$ for $i = 1, 2$. This can be clearly seen from Theorem 5.1.4 as the expected value of the Brownian motion is 0. Next, we turn our attention to $\mathrm{E}((\sigma_t^i)^4)$. This expression will be calculated through simple expansion and evaluation of the terms. As shown by Swishchuk [24],

$$(\sigma_t^i)^2 = e^{-k_i t}(\Delta_i + b_t^i) + \theta_i^2$$

and thus

$$(\sigma_t^i)^4 = ((\sigma_t^1)^2)^2 = (e^{-k_i t}(\Delta_i + b_t^i) + \theta_i^2)^2 \tag{5.3}$$
$$= e^{-2k_i t}(\Delta_i + b_t^i)^2 + 2(\Delta_i + b_t^i)\theta_i^2 e^{-k_i t} + \theta_i^4 \tag{5.4}$$
$$= e^{-2k_i t}(\Delta^2 + 2\Delta_i b_t^i + (b_t^i)^2) + 2(\Delta_i + b_t^i)\theta_i^2 e^{-k_i t} + \theta_i^4. \tag{5.5}$$

Now, taking the expectation of both sides we have

$$\mathrm{E}((\sigma_t^i)^4) = e^{-2k_i t}(\Delta^2 + 2\Delta_i \,\mathrm{E}(b_t^i) + \mathrm{E}((b_t^i)^2)) + 2(\Delta_i + \mathrm{E}(b_t^i))\theta_i^2 e^{-k_i t} + \theta_i^4.$$

The expectation of b_t^i is 0. Swishchuk [24] has also shown that

$$\mathrm{E}((b_t^i)^2) = \gamma_i^2 \left\{ \frac{e^{k_i t} - 1}{k_i}\Delta_i + \frac{e^{2k_i t} - 1}{2k_i}\theta_i^2 \right\}. \tag{5.6}$$

And so equation (5.5) simplifies to

$$\mathrm{E}((\sigma_t^i)^4) = e^{-2k_i t}(\Delta^2 + E((b_t^i)^2)) + 2\Delta_i\theta_i^2 e^{-k_i t} + \theta_i^4 \tag{5.7}$$

and therefore

$$\mathrm{Var}(\sigma_t^i) = \mathrm{E}((\sigma_t^i)^4) - \mathrm{E}^2((\sigma_t^i)^2)$$

is fully known and the integrand is calculable. At last, we have proved the following theorem.

Theorem 5.2.1. *Two assets following the Heston model described in 4.10 may have their continuous-time covariance approximated with*

$$\rho_t \,\mathrm{E}\left(\sqrt{(\sigma_t^1\sigma_t^2)^2}\right) \approx \rho_t\Bigg(\sqrt{\mathrm{E}((\sigma_t^1)^2)\,\mathrm{E}((\sigma_t^2)^2)} - \frac{1}{8}\sqrt{\frac{\mathrm{E}((\sigma_t^2)^2)}{\mathrm{E}^3((\sigma_t^1)^2)}}\,\mathrm{Var}((\sigma_t^1)^2) - \frac{1}{8}\sqrt{\frac{\mathrm{E}((\sigma_t^1)^2)}{\mathrm{E}^3((\sigma_t^2)^2)}}\,\mathrm{Var}((\sigma_t^2)^2)\Bigg).$$

where for $i = 1, 2$

$$\mathrm{E}((\sigma_t^i)^2) = e^{-k_i t}\Delta_i + \theta_i^2,$$
$$\mathrm{E}((\sigma_t^i)^4) = e^{-2k_i t}(\Delta^2 + E((b_t^i)^2)) + 2\Delta_i\theta_i^2 e^{-k_i t} + \theta_i^4$$

with

$$\mathrm{E}((b_t^i)^2) = \gamma_i^2 \left\{ \frac{e^{k_i t} - 1}{k_i} \Delta_i + \frac{e^{2k_i t} - 1}{2k_i} \theta_i^2 \right\}.$$

Recall that we must integrate this expression to determine the realized covariance between S^1 and S^2. Integrating this expression and dividing by T to obtain $\mathrm{Cov}_R(S^1, S^2)$ is most likely impossible analytically, and so approximation methods must be used. Explicitly writing out the fully substituted expressions is exceptionally difficult due to their quickly growing size and complexity, thus we avoid writing out fully substituted expressions and perform the upcoming calculations using MatLab's symbolic computation packages.

Before moving onto the correlation swap fair strike valuation, there is a structure worthy of note in equation (5.6). Namely, recall that $\Delta_i = (\sigma_0^i)^2 - \theta_i^2$ where $(\sigma_0^i)^2$ is the instantaneous variance and θ_i^2 is the mean-reverting level of the asset variance process. Thus Δ_i is a measure of the signed distance of the asset's variance from the long-run asset variance. Equation (5.6) is composed of three notable parts. Firstly, the volatility of the volatility, γ_i is clearly a scaling factor for the variance of the whole expression. Secondly, the first term is scaled by Δ_i, indicating that the variance of the underlying Brownian motion depends on the distance of the asset process's variance from its long-run mean. Thirdly, the final term is scaled by θ_i^2 which indicates the variance of the underlying Brownian motion depends on the size of the long-run mean for the asset's variance process. These statements out of context are already agreeable given common intuitions about commodity prices, but these observations give character to the otherwise messy enigmatic abstractions. In situations such as this fair strike valuation, the excess of notation and long expressions can overshadow many structures which may contribute to building intuition and understanding of the behaviour of asset prices in general.

5.3 Correlation Swaps

The valuation of correlation swaps is very similar to the valuation of covariance swaps, however the expected value is substantially more difficult to obtain. Luckily most of the required derivations are given in the previous section. The correlation swap fair strike is to be derived from equation (1.2),

$$K_{corr} = \mathrm{E}(\mathrm{Corr}_R(S^1, S^2)).$$

the definition of $\mathrm{Corr}_R(S^1, S^2)$ is

$$\mathrm{Corr}_R(S^1, S^2) := \frac{\mathrm{Cov}_R(S^1, S^2)}{\sqrt{(\sigma_R^1)^2}\sqrt{(\sigma_R^2)^2}}.$$

It is clear that another approximation must be relied upon in order to create a workable expression for the expected value of the realized correlation, Salvi and Swishchuk in [20] did exactly this with

$$\mathrm{Corr}_R(S^1, S^2) = \frac{\frac{1}{T}\int_0^T \rho_t \sigma_t^1 \sigma_t^2 dt}{\sqrt{(\sigma_R^1)^2}\sqrt{(\sigma_R^2)^2}} \tag{5.8}$$

and after some work they obtained the approximation

$$\mathrm{E}(\mathrm{Corr}_R(S^1, S^2)) \approx \frac{\frac{1}{T}\int_0^T \rho_t \,\mathrm{E}(\sigma_t^1 \sigma_t^2) dt}{\sqrt{(\mathrm{E}(\sigma_R^1)^2)}\sqrt{\mathrm{E}((\sigma_R^2)^2)}}. \tag{5.9}$$

The the radicands in the denominator are easily determined for $i = 1, 2$ as

$$\mathrm{E}((\sigma_R^i)^2) = \frac{1}{T}\int_0^T \mathrm{E}((\sigma_t^i)^2) dt = \frac{1 - e^{-k_i T}}{k_i T}\Delta_i + \theta_i^2,$$

and the numerator is exactly equal to K_{cov}:

$$\mathrm{E}(\mathrm{Corr}_R(S^1, S^2)) \approx \frac{K_{cov}}{\sqrt{(\mathrm{E}(\sigma_R^1)^2)}\sqrt{\mathrm{E}((\sigma_R^2)^2)}}. \tag{5.10}$$

Thus, we arrive at another theorem

Theorem 5.3.1. *Two assets following the Heston model described in 4.10 may have their continuous-time realized correlation approximated with*

$$\mathrm{E}(\mathrm{Corr}_R(S^1, S^2)) \approx \frac{K_{cov}}{\sqrt{\frac{1-e^{-k_1 T}}{k_1 T}\Delta_1 + \theta_1^2}\sqrt{\frac{1-e^{-k_2 T}}{k_2 T}\Delta_2 + \theta_2^2}}.$$

5.4 Covariance and Correlation Swap Fair Strike Prices

This section is primarily devoted to the integration of the equation in Theorem 5.2.1. Due to the rapidly increasing intractability of these expressions, they are approximated using Taylor polynomial and integration packages available in MatLab. The code is supplied in Appendix 8. Since our functions are all within expected values, their stochastic elements have been handled and the inside functions are smooth and continuous over the interval $(0, T)$. The only possible concern is whether the denominator of the second term of the integrand is 0. This can only happen if at least one of $\mathrm{E}((\sigma_t^i)^2) = 0$ for $i = 1, 2$. Since $\mathrm{E}((\sigma_t^i)^2) = e^{-k_i t}\Delta_i + \theta_i^2$, we can set this equal to zero and determine when this approximation may not be valid:

$$\begin{aligned} \mathrm{E}((\sigma_t^i)^2) &= e^{-k_i t}\Delta_i + \theta_i^2 = 0 \\ \implies e^{-k_i t} &= -\frac{\theta_i^2}{\Delta_i}. \end{aligned}$$

The exponential function is positive for all real numbers t and k_i, θ_i^2 is always nonnegative. Thus a condition for this equality to hold is $\Delta_i = (\sigma_0^i)^2 - \theta_i^2 > 0$, i.e. when the instantaneous variance of the asset, $(\sigma_0^i)^2$ is greater than the mean-reverting level θ_i^2. This condition is likely too relaxed to be usable in practice, especially since $\theta_i^2 > 0$ by assumption. Alternatively, the CIR model will never reach zero if the Feller condition discussed in equation (3.1) holds. In practice, the volatility of an asset can never be non-positive and so $\mathrm{E}((\sigma_t^i)^2) = 0$ is not of practical concern. The CIR model for volatility

remains useful despite the Feller condition being violated in practice and so this is likely to not become an issue. Indeed as seen in section 3, even if the process touches 0 momentarily, it will rebound quickly to become positive again. Thus we press on with our approximation.

Despite the bivariate approximation already being a second-order Taylor approximation, in order to navigate this integral, we must take another second-order Taylor approximation of the integrand around a point within $[0, T]$. Unlike the bivariate approximation, this Taylor approximation will be with respect to the time variable t instead of $(\sigma_t^1)^2$ and $(\sigma_t^2)^2$. This allows for an easy polynomial integration. We note that $a = 0$ would be the best choice to simplify the expressions involved, but the choice $T/2$ may be better to minimize error since $t \in [0, T]$ and the error of a Taylor polynomial increases with distance from a. So the choice of $a = 0$ naturally raises concern about the introduction of large errors into the approximation. Since the expressions will be impossible to write down regardless of the choice of a, very little will be gained by attempting to choose an a that simplifies the expressions. For this reason, the Taylor approximation is taken with $a = T/2$. There is a famous quantity known as the Lagrange error bound which allows us to quantify this error quite handily:

Theorem 5.4.1 (Taylor's Theorem)**.** *Let $f(x)$ be an $n+1$ times continuously differentiable function over an open interval, I containing a, where n is a positive integer. Then for each x in the interval I,*

$$f(x) = \sum_{j=0}^{n} \left(\frac{f^{(j)}(a)}{j!}(x-a)^j \right) + R_n(x)$$

where

$$R_n(x) = \frac{f^{(n+1)}(c)}{(n+1)!}(x-a)^{(n+1)}$$

for some c in between a and x.

Theorem 5.4.2 (Lagrange Error Bound)**.** *Let $f(x)$ be an $n+1$ times continuously differentiable function over an open interval I containing a, where n is a positive integer. Then*

$$R_n(x) \leq \frac{|f^{(n+1)}(c)|}{(n+1)!}|(x-a)^{(n+1)}|$$

is the maximum error possible for a Taylor expansion of degree n about a. Where c is chosen such that it is between x and a, and maximizes $|f^{(n+1)}(c)|$.

The error of these approximations will be discussed later. For now, we apply Theorem 5.4.1 to the approximation in Theorem 5.2.1 to obtain the quantity to be integrated. The first and second terms,

$$\sqrt{\mathrm{E}((\sigma_t^1)^2)\,\mathrm{E}((\sigma_t^2)^2)}$$

and

$$-\frac{1}{8}\sqrt{\frac{\mathrm{E}((\sigma_t^2)^2)}{\mathrm{E}^3((\sigma_t^1)^2)}}\,\mathrm{Var}((\sigma_t^1)^2) - \frac{1}{8}\sqrt{\frac{\mathrm{E}((\sigma_t^1)^2)}{\mathrm{E}^3((\sigma_t^2)^2)}}\,\mathrm{Var}((\sigma_t^2)^2)$$

respectively, are handled individually with different choices of $f(t)$ and then added together to further trivialize the integral enough that a computer can do it using its programmed algorithms for basic integrals and avoid relying on numerical methods. Additionally this will gives us extra versatility with the determination of the error of the approximation with the Lagrange error bound as we may choose the number of Taylor terms for both $f_1(t)$ and $f_2(t)$. For the first term, the choice of $f(t)$ is

$$f_1(t) = \sqrt{\mathrm{E}((\sigma_t^1)^2)\,\mathrm{E}((\sigma_t^2)^2)}, \tag{5.11}$$

and for the second term the choice of $f(t)$ is

$$f_2(t) = -\frac{1}{8}\sqrt{\frac{\mathrm{E}((\sigma_t^2)^2)}{\mathrm{E}^3((\sigma_t^1)^2)}}\,\mathrm{Var}((\sigma_t^1)^2) - \frac{1}{8}\sqrt{\frac{\mathrm{E}((\sigma_t^1)^2)}{\mathrm{E}^3((\sigma_t^2)^2)}}\,\mathrm{Var}((\sigma_t^2)^2). \tag{5.12}$$

The Taylor approximations of the above expressions along with their derivatives are unruly enough that they cannot reasonably be written down.

It is worth noting that even though the expressions are incredibly difficult to write down, they are only polynomials with exceptionally complicated constants. The general form of each Taylor polynomial is given for $l = 1, 2$ as

$$\frac{\rho_t}{T}\left(f_l(T/2) + f_l'(T/2)(t - T/2) + \frac{1}{2}f_l''(T/2)(t - T/2)^2\right).$$

Setting $\rho_t = \rho$ to be a constant, the integration is now easy, set $u = t - T/2$ and thus $du = dt$ which implies that for $l = 1, 2$ representing the two choices of $f(t)$ for the Taylor expansion,

$$\int_0^T \frac{\rho}{T}\left(f_l(T/2) + f_l'(T/2)(t - T/2) + \frac{1}{2}f_l''(T/2)(t - T/2)^2\right) dt \tag{5.13}$$

$$= \int_{-T/2}^{T/2} \frac{\rho}{T}\left(f_l(T/2) + f'(T/2)(u) + \frac{1}{2}f_l''(T/2)(u)^2\right) du \tag{5.14}$$

$$= \frac{\rho}{T}\left(f_l(T/2)T + f_l'(T/2)\left(\frac{T^2}{4} - \frac{T^2}{4}\right) + f_l''(T/2)\frac{T^3}{24}\right) \tag{5.15}$$

$$= \rho\left(f_l(T/2) + f_l''(T/2)\frac{T^2}{24}\right). \tag{5.16}$$

Using symbolic differentiation in MatLab we can obtain the derivatives of $f_1(t)$ and $f_2(t)$ and substitute $t = T/2$. These expressions cannot be written out explicitly due to their length and complexity. Since they can be held in computer memory, we may substitute them freely with values as desired. We arrive at the main results of this paper:

Theorem 5.4.3. *The continuous-time covariance swap fair strike between two assets following the Heston model, S^1 and S^2 can be approximated with*

$$K_{cov} \approx \rho\left(f_1(T/2) + f_1''(T/2)\frac{T^2}{24} + f_2(T/2) + f_2''(T/2)\frac{T^2}{24}\right)$$

where $f_1(t)$ and $f_2(t)$ are given by equations (5.11) and (5.12) respectively.

We can also restate Theorem 5.3.1 in terms of Theorem 5.4.3:

Theorem 5.4.4. *Two assets following the Heston model described in 4.10 may have their continuous-time correlation swap fair strike approximated with*

$$K_{corr} \approx \frac{\rho\left(f_1(T/2) + f_1''(T/2)\frac{T^2}{24} + f_2(T/2) + f_2''(T/2)\frac{T^2}{24}\right)}{\sqrt{\frac{1-e^{-k_1T}}{k_1T}\Delta_1 + \theta_1^2}\sqrt{\frac{1-e^{-k_2T}}{k_2T}\Delta_2 + \theta_2^2}}$$

where $f_1(t)$ and $f_2(t)$ are given by equations (5.11) and (5.12) respectively.

Remark 5.4.5. It is worth noting that the Lagrange error bound for the approximation in Theorem 5.4.3 is of degree 3 in T. This is because the Taylor approximation is taken to the second-order leaving a polynomial error term of degree 3 and then integrated and divided by T. By the power rule for integration, we know that the degree must then increase to 4 and then simplifies down to 3. We take the Lagrange error term and apply the same methods to it as Theorem 5.4.3. For $l = 1, 2$ with the substitutions $u = t - T/2$ and $d_l = c_l - T/2$,

$$R_{2,l}(u) \leq \frac{|f_l^{(2+1)}(d_l)|}{(2+1)!}|(u)^{(2+1)}|$$

By Theorem 5.4.2. Now integrating both sides from $u = -T/2$ to $u = T/2$ (i.e. $t = 0$ to $t = T$) and multiplying by $|\rho|/T$ we have

$$\frac{|\rho|}{T}\int_{-T/2}^{T/2} R_{2,l}(u)du \leq \frac{|\rho|}{T}\int_{-T/2}^{T/2}\frac{|f_l^{(3)}(d_l)|}{3!}|u^3|du \tag{5.17}$$

$$= \frac{|\rho|}{T}\int_0^{T/2}\frac{|f_l^{(3)}(d_l)|}{3!}u^3du + \frac{|\rho|}{T}\int_{-T/2}^{0} -\frac{|f_l^{(3)}(d_l)|}{3!}u^3du \tag{5.18}$$

$$= |\rho|\frac{|f_l^{(3)}(d_l)|}{192}T^3 \tag{5.19}$$

where d_l is the value in $[-T/2, T/2]$ which maximizes $|f_l^{(3)}(d_l)|$ for $l = 1, 2$. Thus this approximation will get significantly less accurate once the expiry time of the swap exceeds $T = 2$ years. Fortunately, there is a large

denominator in this expression and so the error contributed to the valuation of the fair strike of the swaps by this second approximation is expected to be small. This may not be the case if either of $|f_l^{(3)}(d_l)|$ are exceptionally large. It is also worth noting that multiple powers of T may be added by $|f_l^{(3)}(d_l)|$ to the T^3 term, further punishing expiry horizons of over 2 years.

Theorem 5.4.3 is a sum of two second-order Taylor approximations and so we arrive at the following theorem after some simple factoring:

Theorem 5.4.6. *The error contributed from the second set of Taylor approximations in the valuation of the covariance and correlation swap fair strikes is at most*

$$\frac{|\rho|\,T^3}{192}\left(|f_1^{(3)}(d_1)| + |f_2^{(3)}(d_2)|\right)$$

where d_1 and d_2 are values in $[0,T]$ which maximize $|f_1^{(3)}(d_1)|$ and $|f_2^{(3)}(d_2)|$. $f_1(t)$ and $f_2(t)$ are given by Theorem 5.4.3 and $\rho \in [-1,1]$ is the instantaneous correlation between the two assets S^1 and S^2.

Part IV

Numerical Calculation of Covariance and Correlation Swaps

Introduction

This part is dedicated to the application of Theorems 5.4.3 and 5.4.4 to the 2019 crude oil and natural gas data sets. We begin this section with a restatement of the Table 2.1 since it tells us the calibration parameters for the Heston model.

Parameter	Crude Oil	Natural Gas
k	7.9506241	7.4939013
T	1	1
σ_0	0.021161467	0.026680822
θ	0.1140747	0.2068726
γ	1.0490996	3.8696995
α	0.0262925	0.10890697
β	0.9424058	0.86158949
C	0.0000141	0.0000240
dt	1/254	1/254
ξ	7.268077524	5.970607225

Table 5.1: Heston model parameters for one year of daily 2019 crude oil and natural gas futures. The p-values for α, β and C for the crude oil data set are 0.151, $2.24 * 10^{-194}$, and 0.0988 respectively. For the natural gas data set, the p-values are 0.00876, $9.95 * 10^{-44}$, and 0.260 respectively.

In chapter 6 we will observe how the changes in three key parameters, k, θ, and γ may affect our valuation due to the calibration errors discussed in section 8. This analysis consists of plotting the covariance fair strike and correlation fair strike as a function of each parameter while holding

everything else constant. Using this technique we will also be able to build intuition for the behaviour of covariance and correlation swaps based on the value of the parameters.

Next, in chapter 7 we will attempt to address the inaccuracies present in the calibration by proposing three different valuations of the fair strike defined as K, $\tilde{K}$, and $\dot{K}$. K is a direct application of Theorems 5.4.3 and 5.4.4. $\tilde{K}$ and $\dot{K}$ are truncations of the aforementioned theorems which sacrifice accurate error bounds in favour of accurate valuation (in the case of $\tilde{K}$) or sacrifice accurate valuation in favour of accurate error bounds (in the case of $\dot{K}$).

Chapter 6

Effects of changes in k, θ, and γ

The most important parameters are k, θ, and γ as they determine most of the value of the swaps. From the discussion in section 8, we know that there is a high likelihood the parameters have large errors, most notably γ since the peak of its error distribution is far away from 0% error. It will be valuable to see how varying these three parameters affects the fair strike value. For this comparison, all values will be set to those in Table 5.1 while the parameter of interest is given as 1000 values varying between 0% and 1000% of the value listed in the table. This should give a good range of likely values around the errors discussed in appendix 8. This will be carried out for both the 2019 crude oil and 2019 natural gas calibrations, resulting in 12 plots since two swaps are being investigated.

Firstly, it is important to recognize that the fair strike value for a correlation swap should be bounded on the interval $[-1, 1]$. Since the parameters are being varied far outside the bounds of realism while all other parameters are being held constant, it is only natural that this bound is violated in Figures 6.1, 6.2, and 6.3. As is evidenced by Figures 6.1 and 6.2, θ and k only create significant changes when they are close to zero due to the vertical asymptote at zero. There is a negative slope on the top plot of Figure 6.2. This is not present in its natural gas counterpart. The reason for this

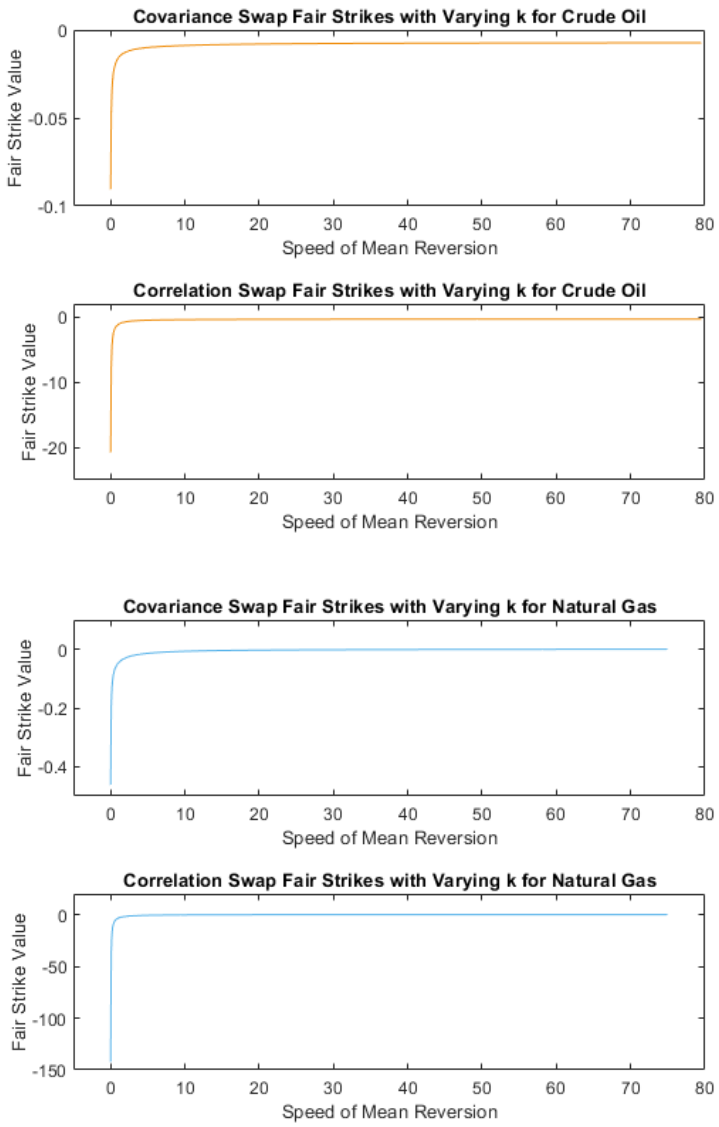

Figure 6.1: Change of value for covariance and correlation swap fair strikes as a function of the changing mean reversion speeds, k_1 and k_2. The top set of plots are from the 2019 crude oil data, the bottom is 2019 natural gas data.

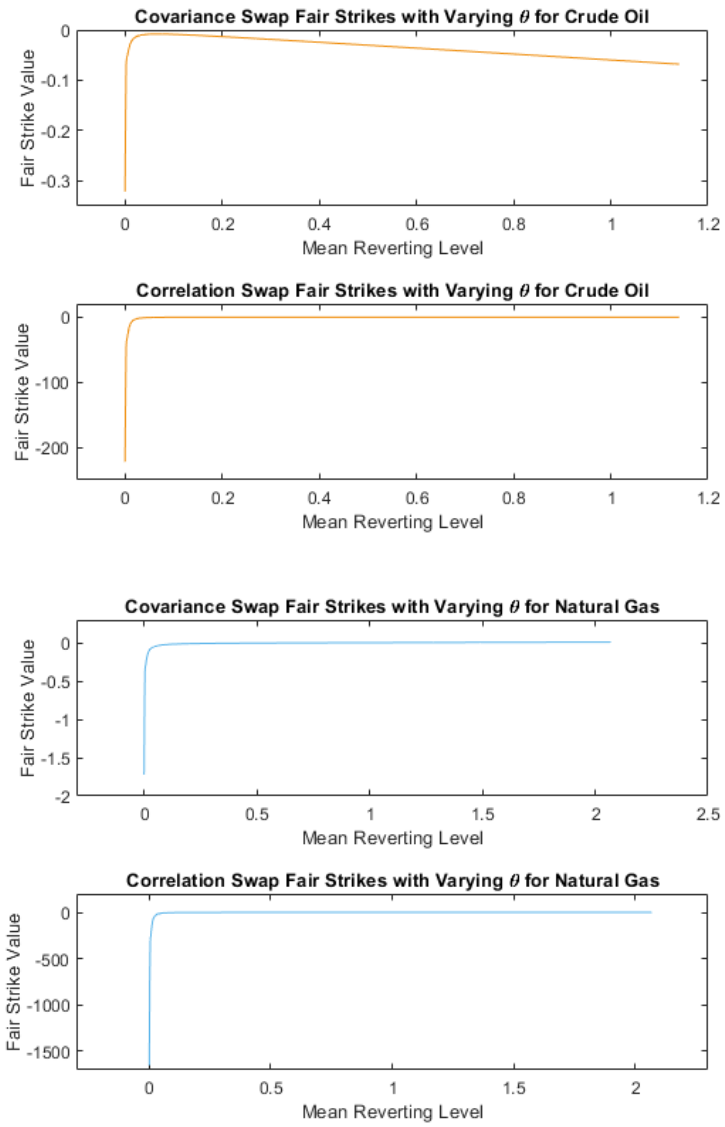

Figure 6.2: Change of value for covariance and correlation swap fair strikes as a function of the changing mean reverting levels, θ_1 and θ_2. The top set of plots are from the 2019 crude oil data, the bottom is 2019 natural gas data.

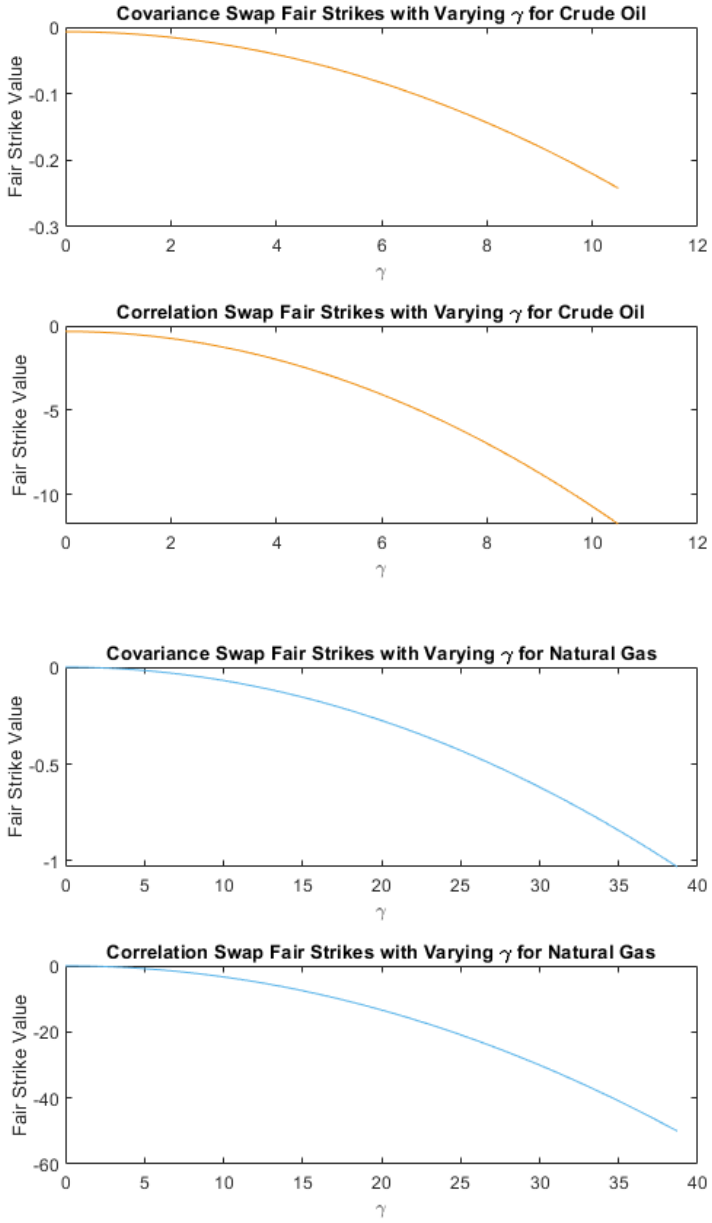

Figure 6.3: Change of value for covariance and correlation swap fair strikes as a function of the changing volatilities of the CIR process, γ_1 and γ_2. The top set of plots are from the 2019 crude oil data, the bottom is 2019 natural gas data.

negative slope is unclear as of the writing of this paper but is very small when taking the scale of the axis into account. Lastly, the variation of γ in Figure 6.3 appears to be the biggest source of sensitivity in the system since we know from appendix 8 that γ has a tendency to be overestimated and that these plots indicate increases in γ lead to strong decreases of swap value.

We note that the swap valuations are negative in all plots except for some small intervals with small γ in Figure 6.3. Since there is likely a large error in γ and all parameters are held constant with exception of the varying parameter in each plot, the negative bias γ inflicts appears to have dominated the valuation. We know that the correlation between the log returns of natural gas and crude oil is given by $\rho = 0.161464948$ and from Table 2.2 the discrete realized correlation for the Heston model was 0.158850823. Thus, the correlation swap fair strike between these two commodities should be near these values, which implies γ is very far off from its true value.

Chapter 7

Fair strike calculations

Theorems 5.4.3 and 5.4.4 give approximations for the fair strikes of covariance and correlation swaps. In the previous chapter, it was demonstrated that γ is likely overestimated. We present two variations of Theorem 5.4.3 in an attempt to mitigate this problem. Recall that Theorem 5.4.3 gives the fair strike approximation as

$$K_{cov} \approx \rho \left(f_1(T/2) + f_1''(T/2)\frac{T^2}{24} + f_2(T/2) + f_2''(T/2)\frac{T^2}{24} \right)$$

where $f_1(T/2) + f_1''(T/2)T^2/24$ is a second order Taylor approximation of $f_1(t)$ and $f_2(T/2) + f_2''(T/2)T^2/24$ is a second order Taylor approximation of $f_2(t)$. $f_1(t)$ and $f_2(t)$ come from the bivariate Taylor approximation of $f(x, y) = \sqrt{xy}$. Thus, by Theorem 5.4.2 we have flexibility on which terms are assigned to the value of the swaps and which terms are assigned to the error estimation. Armed with the knowledge that γ is the main source of error, we aim to avoid using γ in our final value. This is a double-edged sword however since successive terms in a Taylor approximation also contribute to the precision of the valuation. We propose to use the first two terms of the covariance fair strike to value the swaps and let term 3 be the error. This will lead to a poor estimation of the error bound but will give a reasonable value for K_{cov} and K_{corr} since γ will be omitted

from the valuation. Term 4 is omitted for simplicity and since additional precision will not be granted with γ biasing the calculations. The γ-omitted approximations of the fair strike covariance and correlation swaps become

$$\tilde{K}_{cov} \approx \rho \left(f_1(T/2) + f_1''(T/2)\frac{T^2}{24} \pm f_2(z) \right), \tag{7.1}$$

$$\tilde{K}_{corr} \approx \frac{K_{cov}}{\sqrt{\frac{1-e^{-k_1 T}}{k_1 T}\Delta_1 + \theta_1^2}\sqrt{\frac{1-e^{-k_2 T}}{k_2 T}\Delta_2 + \theta_2^2}} \tag{7.2}$$

where z is the value which maximizes $f_2''(t)$ on the interval $[0, T]$. Alternatively, we can omit the use of γ entirely from the error bound and use only term 1 for the value and term 2 for the error approximation.

$$\dot{K}_{cov} \approx \rho \left(f_1(T/2) \pm f_1''(z)\frac{T^2}{24} \right), \tag{7.3}$$

$$\dot{K}_{corr} \approx \frac{K_{cov}}{\sqrt{\frac{1-e^{-k_1 T}}{k_1 T}\Delta_1 + \theta_1^2}\sqrt{\frac{1-e^{-k_2 T}}{k_2 T}\Delta_2 + \theta_2^2}} \tag{7.4}$$

where z is the value which maximizes $f_1''(t)$ on the interval $[0, T]$. We now evaluate Theorems 5.4.3 and 5.4.4; equations (7.1) and (7.2); and equations (7.3) and (7.4) using MatLab's symbolic differentiation package:

$$K_{cov} \approx -0.009137 \pm 1262 \text{ and } K_{corr} \approx -0.4431 \pm 61213,$$

$$\tilde{K}_{cov} \approx 0.003537 \pm 0.01337 \text{ and } \tilde{K}_{corr} \approx 0.1716 \pm 0.6606,$$

$$\dot{K}_{cov} \approx 0.003732 \pm 0.05561 \text{ and } \dot{K}_{corr} \approx 0.1810 \pm 2.697.$$

As we see with these values, we are in a situation where successive Taylor terms increase the error instead of reducing it due to the heavy use of γ in second order and third order terms. We note that in each case, the maximum value for the error term occurred at $t = 0$. K_{cov} and K_{corr} are nowhere near the correct value and the error bounds for our intents and purposes are infinite. $\tilde{K}_{cov}$ and $\tilde{K}_{corr}$ fair much better with realistic values and large, but not ridiculous error bounds. Finally, $\dot{K}_{cov}$ and $\dot{K}_{corr}$ have

larger error bounds than $\tilde{K}$ and also sacrifice precision in the approximation. For this reason, if one were to build a contract with any of the fair strikes listed above, $\tilde{K}_{cov}$ and $\tilde{K}_{corr}$ are recommended. The larger error bounds on $\tilde{K}$ are deceptive because they are likely massively overestimated due to the presence of γ in the error bound estimation. We advise caution for any industrial applications of the methods described in this paper until a more accurate calibration method is found.

Chapter 8

Conclusion

In part I, we showed that the methods of Swishchuk [24] can be applied to 2019 natural gas and crude oil front month futures to approximate the fair strikes natural gas and crude oil volatility and variance swaps in the Heston model. These approximations were shown to be quite different from their corresponding discrete-time realized strikes. The discrete time realized covariance and correlation were also calculated as a benchmark for later in the paper (See Table 2.2). Chapter 3 showed that the spot prices of 2018 and 2019 crude oil and natural gas futures were not strongly mean reverting and more closely resembled a random walk. The p-values from the Augmented Dickey-Fuller and the Phillips-Perron tests were between 0.30 and 0.88, indicating a failure to reject the null hypothesis that the data was not mean-reverting. These results were further affirmed by the mean-reverting algorithmic trading strategy, which used the assumption of mean-reverting spot prices to make trading decisions. Roughly neutral returns across all data sets indicated the spot prices were following a mean-reversion pattern as often as a momentum-based pattern, indicating random walk behaviour.

In part II, we compared the Vasicek, Schwartz one-factor, and Heston models applied to the 2019 data sets against the crude oil volatility index (OVX) and found that the Vasicek model was dramatically outperformed

by the Schwartz one-factor model. The fair strike of the crude oil volatility swap was 3.1926 for the Vasicek model and 0.2177 for the Schwartz one-factor model versus an average OVX value of 0.3384 in 2019. It was also found that the Heston continuous-time model did not perform well at a volatility swap strike of 0.0909. Since the Heston model was expected to be the most precise model of the three, a calibration error analysis was carried out in appendix 8, which explained that the use of γ in the relevant equations introduced significant error because the ML-ARCH approximation of the GARCH(1,1) model tended to overestimate γ by several times its true value.

In part III, we derived closed form approximations for covariance and correlation swaps using several Taylor approximations and methods similar to the ones used by Brockhaus and Long [2] in the continuous-time Heston model. The error of the latter of these approximations was calculated using the Lagrange error bound of a Taylor series.

In part IV, we performed a sensitivity analysis on the main parameters in the valuation of covariance and correlations swaps: k, θ, and γ and found that errors in k and θ had little effects value of the fair strike of both the covariance and correlation swaps provided the values of k and θ were not close to the vertical asymptote at the origin. Significantly different behaviour was found in the plots for γ. An increase in γ lead to a decrease in fair strike value. In the case of the correlation swaps for both data sets (which are bounded within the interval $[-1, 1]$), a relatively small change in γ lead to the value of the swap being reduced below -1. This result combined with the result in appendix 8 which showed that γ was likely to be overestimated by at least 250% indicated that the valuation of covariance and correlation fair strikes for natural gas and crude oil was potentially subject to significant calibration error and that the ML-ARCH calibration approach was insufficient to approximate the GARCH(1,1) model for this application. Since the GARCH(1,1) calibration converges to the Hull and White model

instead of the Heston model, calibration errors dominated the valuations, particularly that of γ. Finally, we used the results from this part to inform ways to avoid this calibration error in the fair strike valuations for the covariance and correlation swaps. Three approximations were presented, K, $\tilde{K}$, and $\dot{K}$ where K was the uninformed fair strike of the contract using the full equation from Theorems 5.4.3 and 5.4.4. $\tilde{K}$ was an informed approximation of the fair strikes avoiding the use of γ in the value and moving it to the error bound, this resulted in the most accurate value for the fair strike of both contracts at the expense of a poor error bound estimation. $\dot{K}$ was a more cautious approximation than $\tilde{K}$ since it avoided the use of γ in both the value and the error bound at the expense of a less accurate value. We then concluded that a more accurate value would be more important than an overly cautious estimation of both the error bound and the strike, and thus $\tilde{K}_{cov} \approx 0.003537 \pm 0.01337$ and $\tilde{K}_{corr} \approx 0.1716 \pm 0.6606$ were the best fair strike values for both the covariance and correlation swaps for the 2019 data sets until a more accurate calibration method is found. These values were reasonably close to the benchmark values given by the discretely realized covariance and correlation from Table 2.2 of 0.02284 and 0.1589 respectively, but we note the covariance approximation is significantly further away from the table value than the correlation approximation. This does not mean the value is incorrect however since the discrete realized approximation is using known data and the approximation is making projections for the fair strike of the contract. It is reasonable to assert that the covariance between natural gas and crude oil futures was simply higher than expected in 2019. Finally, we note that a two-factor volatility model may improve the volatility calculations, e.g., a stochastic equation in place of the constants γ, k, or θ.

Future work for the PhD thesis will include applying the Hawkes process to energy markets.

Bibliography

[1] Thijs van den Berg. "Calibrating the Ornstein-Uhlenbeck (Vasicek) model". In: *Web page http://www.sitmo.com/article/calibrating-the-ornstein-uhlenbeck-model/. View date October 24th* (2011).

[2] Oliver Brockhaus and Douglas Long. "Volatility swaps made simple". In: *RISK Magazine* (2000).

[3] Peter Carr and Roger Lee. "Realized volatility and variance: Options via swaps". In: *Risk* 20.5 (2007), pp. 76–83.

[4] Peter Carr and Roger Lee. "Volatility derivatives". In: *Annu. Rev. Financ. Econ.* 1.1 (2009), pp. 319–339.

[5] Chonnawat Chunhawiksit and Sanae Rujivan. "Pricing discretely-sampled variance swaps on commodities". In: *Thai Journal of Mathematics* 14.3 (2016), pp. 711–724.

[6] José Da Fonseca, Martino Grasselli, and Florian Ielpo. "Hedging (co) variance risk with variance swaps". In: *International Journal of Theoretical and Applied Finance* 14.06 (2011), pp. 899–943.

[7] Kresimir Demeterfi et al. "A Guide to Volatility and Variance Swaps". In: *The Journal of Derivatives* 6.4 (1999), pp. 9–32. ISSN: 1074-1240. DOI: 10.3905/jod.1999.319129. eprint: https://jod.pm-research.com/content/6/4/9.full.pdf. URL: https://jod.pm-research.com/content/6/4/9.

[8] Ashley Ding. "A state-preference volatility index for the natural gas market". In: *Energy Economics* 104 (2021), p. 105625.

[9] Robert J Elliott, Tak Kuen Siu, and Leunglung Chan. "Pricing volatility swaps under Heston's stochastic volatility model with regime switching". In: *Applied Mathematical Finance* 14.1 (2007), pp. 41–62.

[10] Hélyette Geman. "Mean Reversion Versus Random Walk in Oil and Natural Gas Prices". In: Jan. 2007, pp. 219–228. ISBN: 978-0-8176-4544-1. DOI: 10.1007/978-0-8176-4545-8_12.

[11] Steven L Heston and Saikat Nandi. "Derivatives on volatility: some simple solutions based on observables". In: *Federal Reserve Bank of Atlanta WP* 2000-20 (2000).

[12] Y. Hilpisch. *Python for Algorithmic Trading: From Idea to Cloud Deployment*. Python/Finance. O'Reilly Media, Incorporated, 2021. ISBN: 9781492053354. URL: https://books.google.ca/books?id=q4SXzQEACAAJ.

[13] John Hull and Alan White. "The Pricing of Options on Assets with Stochastic Volatilities". In: *The Journal of Finance* 42.2 (1987), pp. 281–300. DOI: https://doi.org/10.1111/j.1540-6261.1987.tb02568.x. eprint: https://onlinelibrary.wiley.com/doi/pdf/10.1111/j.1540-6261.1987.tb02568.x. URL: https://onlinelibrary.wiley.com/doi/abs/10.1111/j.1540-6261.1987.tb02568.x.

[14] Nobuyuki Ikeda and Shinzo Watanabe. *Stochastic differential equations and diffusion processes*. Amsterdam New York Tokyo New York, NY, U.S.A: North-Holland Pub. Co. Kodansha Sole distributors for the U.S.A. and Canada, Elsevier Science Pub. Co, 1989. ISBN: 0444873783.

[15] Antoine Jacquier and Saad Slaoui. *Variance dispersion and correlation swaps*. 2010. DOI: 10.48550/ARXIV.1004.0125. URL: https://arxiv.org/abs/1004.0125.

[16] Joakim Marklund and Olle Karlsson. *Volatility Derivatives–Variance and Volatility Swaps*. 2015.

[17] Joshua McGillivray and Anatoliy Swishchuk. "Covariance and Correlation Swaps in Energy Markets". In: *WILMOTT Magazine* (Submitted 2022).

[18] Sanae Rujivan. "Analytically pricing variance swaps in commodity derivative markets under stochastic convenience yields". In: *Communications in Mathematical Sciences* 19.1 (2021), pp. 111–146.

[19] S&P Dow Jones Indices. *S&P Dow Jones Indices Announces 2021 S&P GSCI Weights*. Nov. 2020. URL: https://www.spglobal.com/spdji/en/documents/indexnews/announcements/20201112-1255559/1255559_spgsci2021cpwindexannouncement.pdf.

[20] Giovanni Salvi and Anatoliy V. Swishchuk. "Covariace and correlation swaps for financial markets with Markov-modulated volatilities". In: *International Journal of Theoretical and Applied Finance* 17.01 (2014). DOI: 10.1142/S021902491450006X. eprint: https://doi.org/10.1142/S021902491450006X. URL: https://doi.org/10.1142/S021902491450006X.

[21] Eduardo S. Schwartz. "The Stochastic Behavior of Commodity Prices: Implications for Valuation and Hedging". In: *The Journal of Finance* 52.3 (1997), pp. 923–973. ISSN: 00221082, 15406261. URL: http://www.jstor.org/stable/2329512.

[22] Artur Sepp. "Pricing options on realized variance in the Heston model with jumps in returns and volatility". In: *The Journal of Computational Finance* 11 (June 2008), pp. 33–70. DOI: 10.21314/JCF.2008.185.

[23] Anatoliy Swishchuk. "Alternatives to Black-76 Model for Options Valuation of Futures Contracts (Lectures' Notes)". In: (Aug. 2020). DOI: 10.13140/RG.2.2.32915.91682.

[24] Anatoliy Swishchuk. "Modeling of variance and volatility swaps for financial markets with stochastic volatilities". In: *WILMOTT Magazine* (Jan. 2004).

[25] Anatoliy V Swishchuk. "Variance and volatility swaps in energy markets". In: *Available at SSRN 1628178* (2010).

[26] Raymond Théoret, Lydie Zabré, and Pierre Rostan. "Pricing volatility swaps: empirical testing with Canadian data". In: *Document de travail- Centre de recherche en gestion* (2002).

[27] Anders B Trolle and Eduardo S Schwartz. "Variance risk premia in energy commodities". In: *The Journal of Derivatives* 17.3 (2010), pp. 15–32.

[28] H Windcliff, Peter A Forsyth, and Kenneth R Vetzal. "Pricing methods and hedging strategies for volatility derivatives". In: *Journal of Banking & Finance* 30.2 (2006), pp. 409–431.

Appendices

Matlab Code

MatLab Code for Calibration

```
clear *;
format long;
%For the GARCH calibration of the Heston model.
%make a garch(a,b) model with a variances and b
    innovations with
%mdl=garch(a,b)
mdl=garch(1,1);

%Load in data to fit to the model (closing prices of 1
     year of crude oil and
%natural gas front month futures.)
CrudeData=readtable('WTICrudeFutures2019.csv').Close;
NGData=readtable('NGFuturesFrontMonth2019.csv').Close;

LENCrude=length(CrudeData)-1;
LENNG=length(NGData)-1;

CrudeLogRet=zeros(LENCrude,1);
NGLogRet=zeros(LENNG,1);

```

```
%Format data in terms of log returns
for i=1:LENCrude
    CrudeLogRet(i)=log(CrudeData(i+1)/CrudeData(i));
end
for i=1:LENNG
    NGLogRet(i)=log(NGData(i+1)/NGData(i));
end

%to fit the data to the model, use estmdl=estimate(mdl
    ,data);
estmdlCrude=estimate(mdl,CrudeLogRet);
estmdlNG=estimate(mdl,NGLogRet);
```

MatLab Code for PP and ADF Tests

```
clear *;
format long;
%For the GARCH calibration of the Heston model.
%make a garch(a,b) model with a variances and b
    innovations with
%mdl=garch(a,b)
mdl=garch(1,1);

%Load in data to fit to the model (closing prices of 1
    year of crude oil and
%natural gas front month futures.)
CrudeData=readtable('WTICrudeFutures2019.csv').Close;
NGData=readtable('NGFuturesFrontMonth2019.csv').Close;

LENCrude=length(CrudeData)-1;
LENNG=length(NGData)-1;
```

```
15
16 CrudeLogRet=zeros(LENCrude,1);
17 NGLogRet=zeros(LENNG,1);
18
19 %Format data in terms of log returns
20 for i=1:LENCrude
21     CrudeLogRet(i)=log(CrudeData(i+1)/CrudeData(i));
22 end
23 for i=1:LENNG
24     NGLogRet(i)=log(NGData(i+1)/NGData(i));
25 end
26
27 %to fit the data to the model, use estmdl=estimate(mdl
       ,data);
28 estmdlCrude=estimate(mdl,CrudeLogRet);
29 estmdlNG=estimate(mdl,NGLogRet);
```

MatLab Code for Simple Moving Average Algorithmic Trading Strategy

```
1 %Uses Luca's Strat to heuristically see if our data is
      mean reverting.
2 %Make sure data is in chronological order, data may be
      imported directly
3 clear *;
4 format long;
5 FILENAME = '2019Crude.xlsx';
6 %Importing the data
7 data=readtable(FILENAME).Close;
8 %removing NaNs
```

```
9  data=rmmissing(data);
10 LEN = length(data);
11 SMAWINDOW = 25; %The size of the window for the simple
       moving average
12 THRESHOLD = 0.02; %The amount of movement required to
       incentivize an investment
13 ISMEANREVERTING=true; %Set to true for mean-reverting
       trading strategy, false for momentum-based.
14
15 %Formatting data into log returns, from this all
       lengths are now LEN-1
16 logRet=log(data(2:LEN)./data(1:LEN-1));
17 %Simple moving average (SMA) calculation and distance
       calcs.
18 SMA = movmean(logRet,[SMAWINDOW-1 0]); %Noncenter,
       only averages from before the 'current time' since
       the future is unknown.
19 dist=logRet-SMA; %Distances between SMA and actual log
       returns.
20 %Discretizing function into indicators for threshold
       crossing to determine
21 %position (short (-1), long (1), or neutral (0) in the
       case of mean reverting).
22 pos = -2*ones(LEN-1,1); %Initialized to impossible
       value to highlight errors.
23 if ISMEANREVERTING
24     for i=1:LEN-1
25         if dist(i)>THRESHOLD %If over SMA then short (
               price will decrease)
26             pos(i)=-1;
```

```
27          elseif dist(i)<=-THRESHOLD %If under SMA then
                long (price will increase)
28              pos(i)=1;
29          else %Case: if within threshold (do nothing,
                price unpredictable)
30              pos(i)=0;
31          end
32      end
33  else
34      for i=1:LEN-1
35          if dist(i)>THRESHOLD %If over SMA then long (
                price will increase)
36              pos(i)=1;
37          elseif dist(i)<=-THRESHOLD %If under SMA then
                short (price will decrease)
38              pos(i)=-1;
39          else %Case: if within threshold (do nothing,
                price unpredictable)
40              pos(i)=0;
41          end
42      end
43  end
44
45  %Shift pos indices forward by one to indicate strat
        implemented next time
46  %period on previous data, multiply by returns to get
        strategy
47  strat = pos(2:LEN-1).*logRet(1:LEN-2);
48  %Plotting cumulative sum to indicate this strategy/
        data over whole dataset.
```

```
49 cumStrat=cumsum(strat);
50 cumLogRet=cumsum(logRet);
51
52 %Creating relevant plots:
53 %Hex Colours: blue=#5bb5eb, orange=#f08e0d
54 tiledlayout(3,1);
55 %Distance plot
56 nexttile
57 time=linspace(0,LEN-2,LEN-1)';
58 SCALAR=ones(LEN-1,1);
59 p1=plot(time,dist); %process plot
60 p1.Color='#5bb5eb';
61 hold on
62 p2=plot(time,THRESHOLD*SCALAR); %upper threshold
63 p2.Color='#f08e0d';
64 p3=plot(time,-1*THRESHOLD*SCALAR); %lower threshold
65 p3.Color='#f08e0d';
66 title({'Distance between log returns and'; ' 25 day
      simple moving average with threshold lines'});
67 xlabel('Time Index (Business Days)');
68 ylabel('Distance');
69 axis([0 LEN min(dist) max(dist)]);
70
71 %position plot
72 nexttile
73 time=linspace(0,LEN-2,LEN-1)'; %Reinitialized for each
       plot since array sizes vary
74 SCALAR=ones(LEN-1,1);
75 p4=plot(time,pos); %position plot
76 p4.Color='#5bb5eb';
```

```
77 title('Recommended daily position for one years of
       data');
78 xlabel('Time Index (Business Days)');
79 ylabel({'Position:'; 'Long (1),'; 'Short (-1),'; '
       Neutral (0)'});
80 axis([0 LEN -1 1]);
81
82 %Returns plot
83 nexttile
84 MINLR=min(cumLogRet);
85 MINSTRAT=min(cumStrat);
86 ABSMIN=min(MINLR,MINSTRAT);
87 MAXLR=max(cumLogRet);
88 MAXSTRAT=max(cumStrat);
89 ABSMAX=max(MAXLR,MAXSTRAT);
90
91 time = linspace(0,LEN-1,LEN-2)';
92 p5=plot(time,cumLogRet(2:LEN-1)); %Asset returns
93 p5.Color='#f08e0d';
94 hold on
95 p6=plot(time,cumStrat); %Strategy returns
96 p6.Color='#5bb5eb';
97 title('Data returns versus strategy returns for one
       year of data')
98 xlabel('Time Index (Business Days)');
99 ylabel('Returns');
100 axis([0 LEN ABSMIN ABSMAX]);
101 legend({'Asset Returns','Strategy Returns'},'Location'
       ,'northwest')
```

MatLab Code for Paramater Error Distributions

```
%Simulate Heston model and estimate paras with MLE
clear *;
k = 8;
th = 0.11;
gam = 1;
mu = 0.2;
hest = heston(mu,k,th,gam,'StartState',[65;0.27]);
ITER = 10000;
DAYS = 2540;
dt=1/DAYS;
%These constants are not calibrated values, they
    determine the index of an
%array.
ALPHA=1;
BETA=2;
CONST=3;

for i=1:ITER
    %Create process
    [S,t,z]=simByEuler(hest,DAYS,'DeltaTime',dt);
    t=t(1:length(t)-1);
    LEN_S=length(S)-1;
    %Treat S as data and perform calibration
    gar=garch(1,1);
    %Format data in terms of log returns
    variances=S(:,2);
    S=real(S(:,1));
```

```
27      for j=1:LEN_S
28          S(j)=log(S(j+1)/S(j));
29      end
30      S=S(1:length(S)-1); %Something odd happens with
            the last value.
31      %Estimate alpha, beta, gamma in GARCH(1,1), write
            to array
32      estGARCH(i)=estimate(gar,S,'Display','off');
33      paras(ALPHA,i)=estGARCH(i).ARCH{1};
34      paras(BETA,i)=estGARCH(i).GARCH{1};
35      paras(CONST,i)=estGARCH(i).Constant;
36  end
37  %Parameter calculations
38  estTh  = paras(CONST,:)./(dt.*(1-paras(ALPHA,:)-paras(
        BETA,:)));
39  estK   = (1-paras(ALPHA,:)-paras(BETA,:))./dt;
40  estGam = paras(ALPHA,:).*((kurtosis(S)-1)./dt).^(1/2);
41  %Error calculations
42  thErrors  = 100*(estTh-th)/th;
43  kErrors   = 100*(estK-k)/k;
44  gamErrors = 100*(estGam-gam)/gam;
45
46  %making the error plots readable, since errors can be
        on the order of 10^7
47  truncatedThErrors=thErrors;
48  DEL_THIS=99999999;
49  for i=1:length(thErrors)
50      if abs(thErrors(i))>3000
51          truncatedThErrors(i)=DEL_THIS;
52      end
```

```
53 end
54 truncatedThErrors=truncatedThErrors(truncatedThErrors
      ~=DEL_THIS);
55
56 truncatedKErrors=kErrors;
57 for i=1:length(kErrors)
58     if abs(kErrors(i))>3000
59         truncatedKErrors(i)=DEL_THIS;
60     end
61 end
62 truncatedKErrors=truncatedKErrors(truncatedKErrors~=
      DEL_THIS);
63
64 truncatedGamErrors=gamErrors;
65 for i=1:length(gamErrors)
66     if abs(gamErrors(i))>3000
67         truncatedGamErrors(i)=DEL_THIS;
68     end
69 end
70 truncatedGamErrors=truncatedGamErrors(
      truncatedGamErrors~=DEL_THIS);
71
72 %Plots
73 BINS=ITER; %alternate option
74 BIN_WIDTH=50;
75 figure();
76 histogram(truncatedThErrors,'BinWidth',BIN_WIDTH,'
      Normalization','probability');
77 title('Theta estimation errors for 10 years of
      simulated data');
```

```
78 xlabel('Error (%)');
79 ylabel('Probability');
80 figure();
81 histogram(truncatedKErrors,'BinWidth',BIN_WIDTH,'
       Normalization','probability')
82 title('K estimation errors for 10 years of simulated
       data');
83 xlabel('Error (%)');
84 ylabel('Probability');
85 figure();
86 histogram(truncatedGamErrors,'BinWidth',BIN_WIDTH,'
       Normalization','probability')
87 title('Gamma estimation errors for 10 years of
       simulated data');
88 xlabel('Error (%)');
89 ylabel('Probability');
90 figure();
91 plot(t,S);
```

MatLab Code for Symbolic Taylor Approximation and Differentiation

```
1 %Theorems from ch8 with bivariate taylor approx
       instead of BL approx
2 clear *;
3 syms k1 k2 d1 d2 Eb1sq Eb2sq th1 th2 t T gam1 gam2 rho
       s01 s02
4 %---
5 %LEGEND
6 %k1 k2 are respective speeds of mean reversion
```

```
%d1 d2 stand for delta_1 and delta_2 are the
    difference between short run
%variance and theta1^2 or theta2^2
%Eb1sq Eb2sq are expected values of respective squared
    BMs
%th1 th2 are the mean reversion level
%t is the time variable we are integrating across from
    0 to T
%gam1 and gam2 stand for gamma_1 and gamma_2 and are
    the respective volatilities of the volatilities
%---
%Second order Taylor approximation for the second term
    of the integrand
%after integration and simplification
Eb1sq=gam1^2*(d1*(exp(k1*t)-1)/(k1)+th1^2*(exp(2*k1*t)
    -1)/(2*k1));
Eb2sq=gam2^2*(d2*(exp(k2*t)-1)/(k2)+th2^2*(exp(2*k2*t)
    -1)/(2*k2));
%The expected value of the fourth and second moments
    of sigma1 and sigma2
Es14=exp(-2*k1*t)*(d1^2+Eb1sq)+2*exp(-k1*t)*d1*th1^2+
    th1^4;
Es24=exp(-2*k2*t)*(d2^2+Eb2sq)+2*exp(-k2*t)*d2*th2^2+
    th2^4;
Es12 =exp(-k1*t)*d1+th1^2;
Es22 =exp(-k2*t)*d2+th2^2;
%Variances of sigma1^2 and sigma2^2
Vars12=Es14-Es12^2;
Vars22=Es24-Es22^2;
%Quotients
```

```
27 q1=Es22/Es12^3;
28 q2=Es12/Es22^3;
29 %Putting it all together for the bivariate taylor
       approximation
30 f1=(Es12*Es22)^(1/2);
31 f2=-1/8*(sqrt(q1)*Vars12+sqrt(q2)*Vars22);
32
33 d1f1=diff(f1,t,1);
34 d1f2=diff(f2,t,1);
35 d2f1=diff(f1,t,2);
36 d2f2=diff(f2,t,2);
37
38 taylorf1   =subs(f1,t,T/2);
39 taylorf2   =subs(f2,t,T/2);
40 taylord1f1=subs(d1f1,t,T/2);
41 taylord1f2=subs(d1f2,t,T/2);
42 taylord2f1=subs(d2f1,t,T/2);
43 taylord2f2=subs(d2f2,t,T/2);
44
45 kcov=rho*(taylorf1+taylord2f1*T^2/24+taylorf2+
       taylord2f2*T^2/24);
46
47 %Spacing is deliberate to help avoid errors in
       misplacing values
48 old1={k1,T,d1,th1,gam1,k2,d2,th2,gam2,rho};
49 new1={7.95062408,1,(0.02116147^2-0.11407472^2)
       ,0.11407472,1.04909960,7.49390125,(0.02668082^2-0.20687263^2)
       ,0.20687263,3.86969947,0.161464948};
50
51 covRStrike=max(abs(double(subs(kcov,old1,new1))))
```

```
52
53 syms E1 E2
54 E1=(1-exp(-k1*T))*d1/(k1*T)+th1^2;
55 E2=(1-exp(-k2*T))*d2/(k2*T)+th2^2;
56
57 corrR=kcov/(E1*E2)^(1/2);
58 corrRStrike=max(abs(double(subs(corrR,old1,new1))))
```

Calibration Error Analysis

Calibration Error Analysis

An underlying issue appears to be present for all continuous-time calculations using the Heston model in this paper. The calibration of the mean-reverting CIR process in the Heston model is difficult to do accurately. The method involves using maximum likelihood estimation to approximate the GARCH(1,1) model. Since the variances are mean reverting, there is an inherent interplay between the speed of mean reversion (k) and the volatility of the variances (γ). When γ is high relative to k, the mean-reversion is unable to act effectively enough to avoid being overshadowed by γ. When γ is low relative to k, strong mean reversions can make k well pronounced but at the expense of overshadowing γ. Moreover, these two parameters can cause problems in estimating θ, the mean-reverting level as well. All of this leads to remarkably high errors in the maximum likelihood approach. Interestingly, these errors are almost always overestimations. One can observe this phenomenon through simulation methods. Unfortunately, since the Feller condition is regularly violated, simulating the Heston model is problematic. The Feller condition ensures the CIR process never reaches 0, but since the Euler stochastic differential equation discretization method relies on small timesteps (as do most discretizations of SDEs, virtually by definition), with a violated Feller condition, it is likely the simulated CIR process not only reaches zero but becomes negative, resulting in complex

values entering the calibrations. A simple way to fix this problem is to simply take the real component. This is far from ideal, but there are not many other viable options. In an attempt to quantify and bound the error introduced to θ, γ, and k, a simulation approach is presented here.

We will simulate several thousand Heston processes using the values from Table 2.1 as the starting parameters. The MatLab code for this can be found in Appendix 8. Although these values are likely far off from properly calibrated values, they are still the only valid jumping-off point. Since the 2019 crude oil dataset did not violate the Feller condition, we will use those values (approximately). r can be found by averaging 52-week treasury bills from the U.S. Department of the Treasury. We set the parameters to the following values:

1. $k = 8$,
2. $\theta = 0.11$,
3. $\gamma = 1$,
4. $r = 0.02$,
5. $dt = 1/254$,

The initial value of the process is set to the average value of the crude oil futures closing price, \$65. The initial value for the CIR process is set to $\sigma_0 = 0.27$, the instantaneous volatility of the futures prices. The simulations provide 254 days of data, as this is the size of the 2019 data set.

The approach is to simulate the Heston process and calibrate according to the resulting data. Since the parameters are known, the calibrated parameters can be compared with the simulation parameters. This allows us to calculate the error in the calibrations and obtain intuition of how well the ML-ARCH approximation of the GARCH(1,1) model calibrates the parameters. The results are shown in Figures 1, 2, and 3. Note that

the parameters occasionally produced errors in excess of $10^7\%$, and so any errors greater than 3000% have been removed to prevent the horizontal axis from stretching to unreasonable scales, limiting the visibility of the distribution. Probability values are determined based on the remaining values.

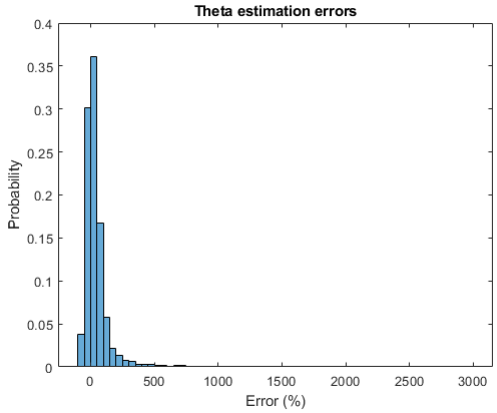

Figure 1: 2019 crude oil data Heston simulation calibration error results for θ after 10000 calibrations. Probability values are determined based on the remaining 9301 values. 699/10000 calibrations for θ were in excess of 3000% error. Each bin width is 50%.

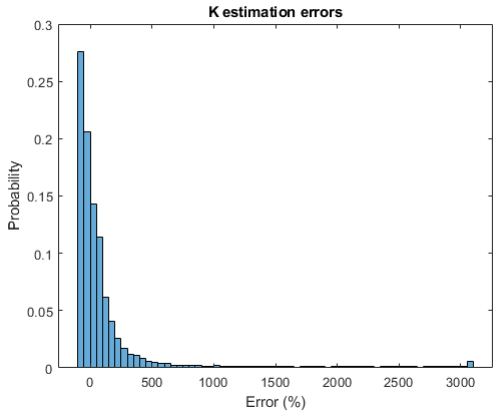

Figure 2: 2019 crude oil data Heston simulation calibration error results for k after 10000 calibrations. Each bin width is 50%.

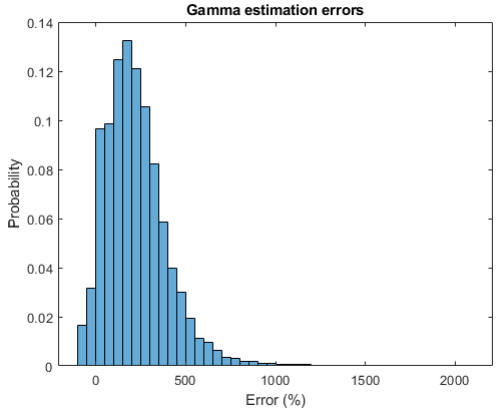

Figure 3: 2019 crude oil data Heston simulation calibration error results for γ after 10000 calibrations. Each bin width is 50%.

From these histograms, it is clear that the error in the calibration is of great significance. The errors frequently exceed 500% and in the case of the γ parameter, is almost 7 times more likely to have an error of 200% than an error of $0 - 50\%$. In fact, none of the peaks exceeds a 0.4 probability of having less than 50% error. We now repeat this process for $dt = 1/2540$ to determine if small sample size or slow convergence issues are a significant source of the large errors.

The behaviour of the data with a resolution 10 times higher is virtually identical to the data with $dt = 254$. There are also significantly fewer values being omitted due to errors over 3000% for θ. The peaks of Figures 4 and 5 are slightly higher at 43% and 38% respectively indicating the precision is increasing with higher sample size, but the distributions have not changed enough to suggest sample size is the main problem with the calibration. Therefore, if one is to use this in industrial applications, it will be valuable to pursue an approximation to the GARCH(1,1) model that is not reliant on maximum likelihood estimation. Curiously, a small node has appeared in Figure 6, this is likely a statistical fluctuation, but more computing power

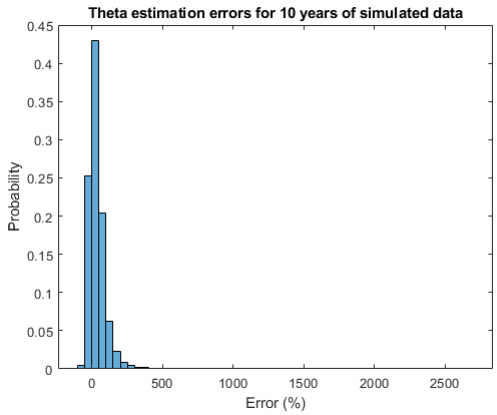

Figure 4: 2019 crude oil Heston simulated calibration error results for θ after 10000 calibrations with $dt = 1/2540$. Probability values are determined based on the remaining 9643 values. 357/10000 calibrations for θ were in excess of 3000% error. Each bin width is 50%.

is needed to pursue this idea. We will continue using ML-GARCH for the remainder of this paper, but we note that significant errors will be present due to the calibration.

This is compelling evidence for why the variances and volatilities from Tables 2.2 and 4.6 are outperformed so dramatically by the discrete Heston calculations. In section 7, the value of the swaps are very close to what one would anticipate them to be, but the error bound calculation involves γ whereas the value only relies on θ and k, indicating θ and k are likely fairly accurate, but γ appears to have been misestimated. Ding in [8] indicated that GARCH models for natural gas volatilities are common due to the auto-regressive behaviour of the spot prices, but typically rely on variants such as EGARCH (Exponential GARCH) and TGARCH (Threshold GARCH) to capture the additional nuance that the GARCH model may miss. In this paper, we use a GARCH(1,1) model for both the crude oil and natural gas calibrations. To improve accuracy, one may choose different models for each commodity based on a more informed statistical analysis of the behaviours of these processes. A good discussion on these calibrations

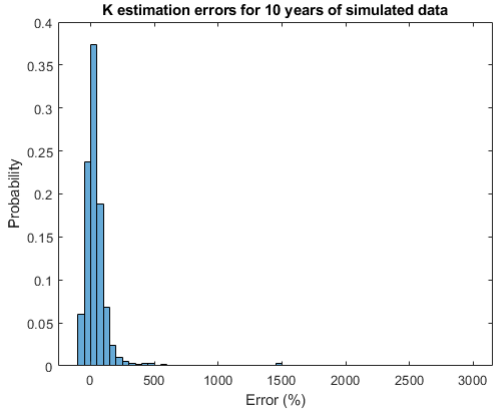

Figure 5: 2019 crude oil data Heston simulated calibration error results for k after 10000 calibrations with $dt = 1/2540$. Probability values are determined based on the remaining 9945 values. 55/10000 calibrations for k were in excess of 3000% error. Each bin width is 50%.

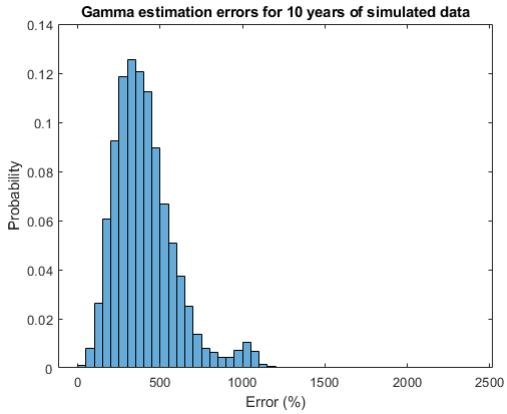

Figure 6: 2019 crude oil data Heston simulated calibration error results for γ after 10000 calibrations with $dt = 1/2540$. Each bin width is 50%.

can be found in [16].